UCRL-9691

UNIVERSITY OF CALIFORNIA

Ernest O. Lawrence Radiation Laboratory

BERKELEY, CALIFORNIA

DISCLAIMER

Research and Development

UCRL-9691
UC-34 Physics Distribution
TID-4500 (16th Ed.)

UNIVERSITY OF CALIFORNIA

Lawrence Radiation Laboratory
Berkeley, California

Contract No. W-7405-eng-48

CHARGE-EXCHANGE SCATTERING OF POSITIVE K MESONS ON DEUTERONS

Wonyong Lee

(Thesis)

May 19, 1961

Printed in USA. Price $1.25. Available from the
Office of Technical Services
U. S. Department of Commerce
Washington 25, D.C.

CHARGE-EXCHANGE SCATTERING OF POSITIVE K MESONS ON DEUTERONS

Contents

UCRL-9691

CHARGE-EXCHANGE SCATTERING OF POSITIVE K MESONS ON DEUTERONS

Wonyong Lee

Lawrence Radiation Laboratory
University of California
Berkeley, California

May 19, 1961

ABSTRACT

The 15-inch deuterium bubble chamber of the Lawrence Radiation Laboratory was exposed to six different momenta of a highly separated K^+—meson beam. An analysis of the K^+- meson—deuteron charge-exchange scattering process has been completed. The total cross sections of K^+-meson—deuteron charge-exchange scattering are $1.0^{+0.4}_{-0.3}$, 2.7±0.4, 3.1±0.4, 6.5±0.6, 6.7±0.6, and 6.6±0.7 mb for K^+ kinetic energies in the laboratory system of 52±17, 100±13, 127±11, 230±11, 315±6, and 456±5 Mev, respectively.

Differential cross sections were measured at four different energies and a phase-shift analysis was carried out. In the analysis the T = 1 phase shift was assumed to be pure S wave. For the T = 0 phase shift SP and SPD fits were made. For the SP fit two sets of phase shifts were obtained for the T = 0 amplitude. In addition, each set has two different solutions corresponding to the Fermi-Yang ambiguity. The two different sets of phase shifts give considerably different K^+-d total cross sections. On this basis, one of the sets was discarded; the remaining set fits the data reasonably well and shows a smooth variation with momentum in the K^+-meson—neutron c.m. system. For the SPD fit in the T = 0 amplitude, two sets of phase shifts were obtained that were identifiable with the two sets of phase shifts in the SP fit with a small D-wave contribution added. In addition, one new set of phase shifts was obtained. Errors in the SPD fit were quite large, and it was concluded that the present data are not statistically accurate enough to determine the five parameters involved here.

In the analysis the elementary differential cross section was expanded into the partial waves with the aid of the impulse and closure approximations. The generalized Pauli principle for two outgoing protons was taken into account in this derivation, but higher-order terms due to multiple scattering, the final proton-proton interaction, and the mass differences were not. These higher-order terms were taken into consideration to the extent of not using the experimental data in the forward direction where the higher terms might be large for the phase-shift analysis.

UCRL-9691

CHARGE-EXCHANGE SCATTERING OF POSITIVE K MESONS ON DEUTERONS

Wonyong Lee

Lawrence Radiation Laboratory
University of California
Berkeley, California

May 19, 1961

I. INTRODUCTION

Below the π-meson production threshold the K^+ meson, in contrast to the K^- meson, interacts strongly with nucleons in only three processes. These three processes can be described by the Coulomb scattering amplitude and the two charge-independent scattering amplitudes M_0 and M_1, corresponding to the total T spin 0 and 1, respectively. Here we will assume that the spin of a K meson is 0 and that $K^+ - K^0$ is a T-spin doublet.

In the pion-nucleon system, the interaction was also expressed by two charge-independent scattering amplitudes and by the Coulomb scattering amplitude. These two charge-independent amplitudes have been investigated by studying the π^+-proton and the π^--proton elastic scattering processes directly. The π-neutron interaction was also investigated by using deuteron targets, but there it was an experimental test of the phenomenological approximations one employs in dealing with deuteron targets.

In the investigation of K^+-meson interactions with nucleons, the scattering amplitude M_1 has been studied in K^+-meson-proton elastic scattering experiments. A knowledge of the M_0 scattering amplitude is, however, hard to obtain, unlike the π-nucleon case. One way is to do the experiment with a K^0 beam, but this is, at present, still a difficult task. Another way is to study the K^+-n interaction. The study of the charge-exchange scattering of K^+ mesons on a deuteron is perhaps the most promising way of learning about the T = 0 amplitude; here there is absolutely no doubt that the K^+ mesons interacted with a neutron. Experimentally, the charge-exchange events are easy to identify when there is a subsequent decay of the K^0 meson. Theoretically, it is easier to deal with because there is no interference term with any other kind of process, as there would be if one studied K^+-n elastic scattering. However, it is not free of theoretical uncertainties, as we will see.

Experimental knowledge of the charge-exchange events has heretofore come from the emulsion experiments, but the information obtained was qualitative because of the well-known difficulties in this technique. The 15-inch deuterium bubble chamber of the Lawrence Radiation Laboratory was exposed to six different momenta of a highly separated K^+-meson beam. An analysis of a K^+-d charge-exchange scattering has been completed, and here we discuss the total cross sections at six different incident K^+-meson momenta, and the differential cross sections at four different incoming momenta.

A partial-wave expansion of the differential cross sections was made with the aid of the impulse and closure approximations. This expansion contains phase shifts as parameters, which depend upon the characteristics of the interaction. A search for these parameters was programmed for both the IBM 704 and 709 machines. The program made use of the method of gradient descent from randomly selected points.

Our justification for using the impulse and closure approximations comes mainly from the experimental evidence, as will be shown. Correction terms due to the final proton-proton interactions, multiple scattering, and the K^+-K^0 mass difference were neglected in the differential-cross-section equation we used for the phase-shift analysis. However, we do take into account these correction terms to the extent of not using the experimental data for the phase-shift analysis in the forward angular region, where the correction terms may be large.

There are four main sources of error in our calculated phase shifts: the first source, due to statistics, is perhaps the largest of all and was calculated by our error program, which used the usual error-matrix analysis. The second source comes from our assumption that the T = 1 state is pure S wave. This assumption is based on the recent experiments on K^+-p elastic scattering. The third source is from the theoretical treatment; that is, the impulse and closure approximations. The last source is due to neglect of higher partial waves, which—though small—may not be zero.

II. EXPERIMENTAL PROCEDURES

Beam Setup[1]

A platinum flip target was placed in the north tangent tank of the Bevatron. Positive K mesons emerging from this target at 30 deg from the direction of the circulating 6.0-Bev/c proton beam were momentum-analyzed and separated by velocity separators, as shown in Fig. 1. The vacuum of the Bevatron was extended through the system to the first slit. The present arrangement is different from a similar one described recently[2] in that the two bending magnets, properly shimmed, also served as vertical focusing elements. This arrangement resulted in reduction of the vertical chromatic aberration of the system. Velocity separation was achieved by crossing electric and magnetic fields; thus the particle with desired velocity was undeflected, whereas the undesired ones were deflected upward or downward according to their masses. The optical effects of the system are shown schematically in Fig. 2. Resolution curves at the two design momenta of 642 and 812 Mev/c are shown in Fig. 3. At 642 Mev/c the estimated background of lighter particles (pions, muons, and electrons) was $\lesssim 0.5\%$. At 812 Mev/c the background was approx 10%. Immediately in front of the chamber, provision was made for the insertion of a momentum degrader to permit a variation of the beam momentum in the chamber. The beam momenta to which the bubble chamber was exposed were 230, 330, 377, 530, 642, and 812 Mev/c. The actual momentum dispersions in the chamber were $\approx 0.7\%$ for both design momenta. This was accomplished with a wedge-shaped absorber behind the second slit. The K^+-meson fluxes in the chamber were 10 and 25 per 10^{11} protons on target at 642 and 812 Mev/c, respectively.

Scanning and Measurement

A total of 71,370 frames were accepted as being good frames for the average momenta of 230, 330, and 530 Mev/c. A good frame was defined as one in which there were either K^+ mesons or some background in the chamber, indicating that the Bevatron beam was on and the chamber was operating properly, and also as a frame in which at least two of the four views were acceptable.

The accepted fiducial volume was ≈ 20 cm long by ≈ 23 cm wide, as seen in View 1. Because all criteria for acceptance were imposed on the tracks as they were seen in View 1, it was required that View 1 always be one of the acceptable views. The criteria for the selection of the fiducial volume were essentially to avoid poorly illuminated or insensitive areas of the chamber, and to allow for extra space to observe the K^0 decay. In addition to the fiducial volume criterion, at 530 Mev/c the incoming track was required to have a projected angle within ± 10 deg of the nominal beam direction. This additional criterion, which helped to eliminate most of the background comtamination at 530 Mev/c, could not be imposed at the lower momenta because of the angular dispersion of the beam caused by the additional amount of absorber in the primary K^+-meson beam. At the lower energies, however, the difference in ionization and curvature enables one to distinquish between K^+ mesons and other particles in the chamber.

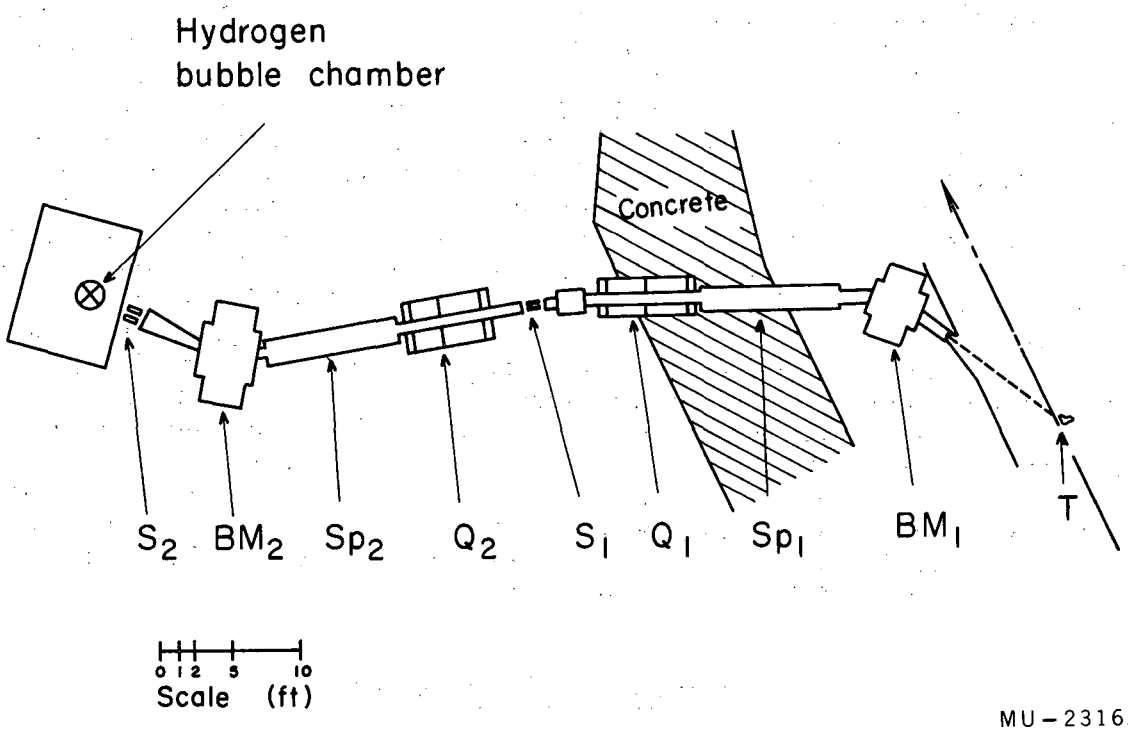

Fig. 1. Schematic plan view of the arrangement of the optical components used to obtain the K^+-meson beam. Here T is the platinum target inside the Bevatron, BM are bending magnets, SP are velocity spectrometers, Q are quadrupole lenses which focus the beam from source to slit, and S are the defining slits.

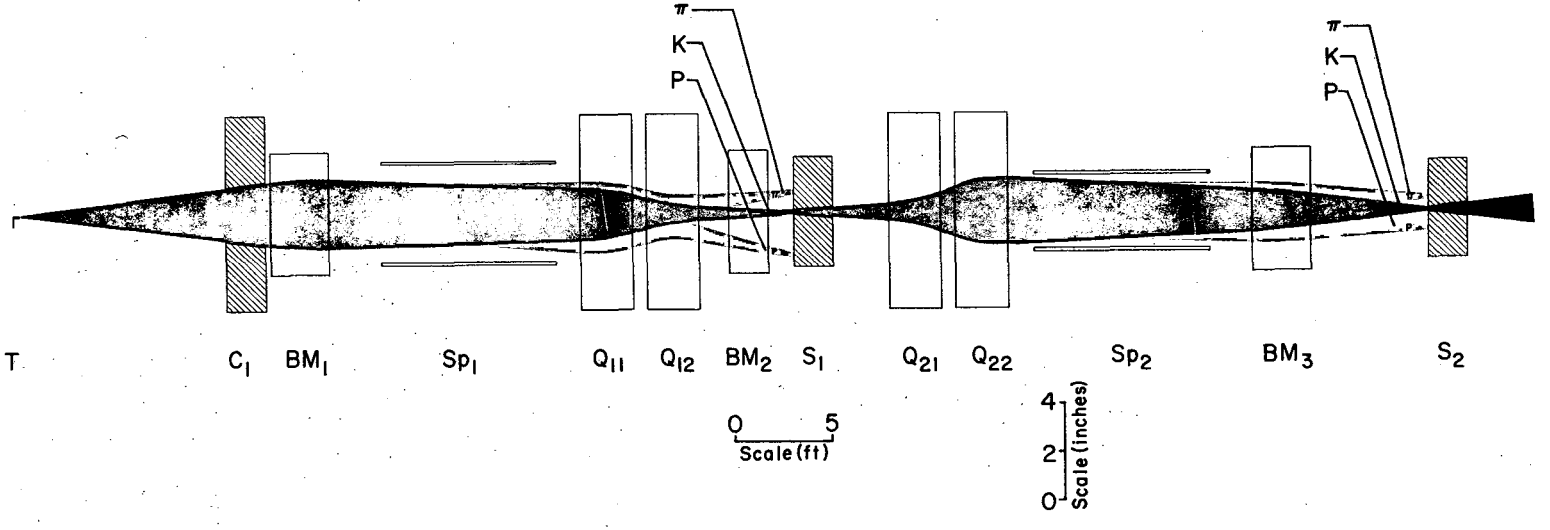

Fig. 2. Vertical section along the beam, showing the detailed action of the optical components. The shaded area is the outline of the beam. The legend is the same as for Fig. 1.

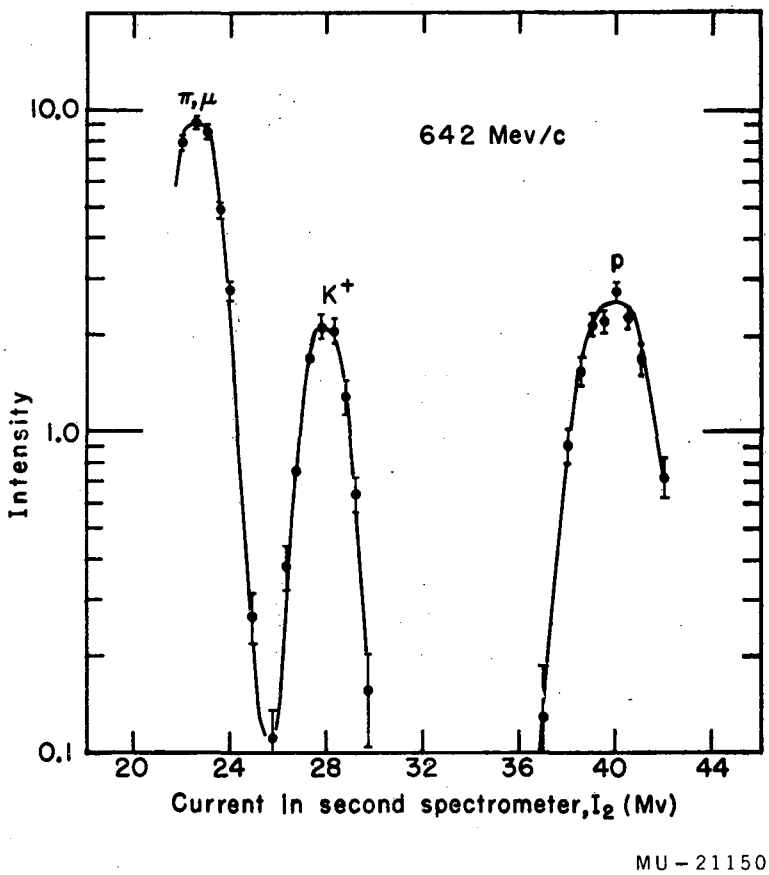

Fig. 3a. Beam intensity transmitted by the second slit versus magnetic field in the second spectrometer. The field strength depended linearly upon the voltage across a voltmeter shunt attached to the magnet coils of the spectrometer. This voltage was experimentally measured and is the abscissa in the plot. The composition of the beam is shown at the momentum for which the system was designed: 642 Mev/c.

Table I. The number of frames for each energy and the number of frames rescanned, along with the efficiency for the detection of the charge-exchange events with neutral K-meson decay through its charged mode

p (Mev/c)	No. of good frames	No. of frames rescanned	Efficiency (%)
230	35,167	18,505	88
330	17,206	17,206	99
530	18,997	10,518	97

Events identified as charge exchange were spatially reconstructed from measurements in two stereo views (Franckenstein measurements), and each track momentum was obtained from the curvature measurements (PANG program).[3]

Not all quantities can be measured equally well. If, at a vertex, all quantities but one are measured well, the poorly measured one is inferred more accurately from the kinematical constraints of energy and momentum conservation. When one of the particles at the vertex is not seen, again its momentum may be inferred from the kinematical constraints. For these purposes and others to be described below, the KICK program was used.[4] In essence this program searches for the maximum of a likelihood function involving the measured quantities, the constraints of momentum and energy conservation, and a hypothesis on the particles taking part in the events. This likelihood function is assumed to be the usual χ^2 distribution function, and its maximization corresponds to minimizing the χ^2. Usually, if χ^2 is reasonable, the given hypothesis is assumed to be good, provided no other hypotheses give reasonable χ^2. The final fitted quantities obtained are naturally more reliable than the measured ones determined by the PANG program.

III. EXPERIMENTAL RESULTS

The beam momenta to which the 15-inch bubble chamber was exposed were 230, 330, 377, 530, 642, and 812 Mev/c. Three of these six momenta—377, 642, and 812 Mev/c—were experimentally analyzed at UCLA, and the other three at Berkeley. We discuss the experimental procedures of only the three momenta analyzed at Berkeley. For the sake of completeness, we present the results of the UCLA group wherever our results are summarized, and discuss all the data when we make the phase-shift analysis. (Preliminary results of this work were reported by Harold K. Ticho at the 1960 Rochester Conference. [5])

Total Cross Sections

The mean free K_1^0 path length produced by incident K^+ mesons of momenta 230, 330, and 530 Mev/c are always less than 1.4, 2.0, and 3.2 cm, respectively. Our fiducial volume gave us a probability of less than 2% that the K_1^0 would not decay anywhere in the entire chamber picture. This 2% was obtained by plotting the number of K_1^0 decays versus time of flight in the rest frame. Given the mass and half life of the K_1^0, we obtained the number of events we should have seen by a least-squares fit. Because of the large statistical errors involved, this slight error is neglected.

Since we made no attempt to look at those events of the charge-exchange interaction in which the K^0 did not decay in the chamber by a two-charged-pion decay mode, we consider the probability that a two-charged-pion decay mode of the K_1^0 is 2/3 of the total decay rate of K_1^0 (or 1/3 of the total charge-exchange events). The latest experimental branching ratio $(K_1^0 \rightarrow \pi^+ + \pi^-)/$ (all K^0) is reported to be 0.339 ± 0.020. [6]

In Table II we list the total cross sections at six different energies between 52 and 456 Mev, along with the number of events we observed at each energy. In Fig. 4 we show the total cross sections as a function of K^+ kinetic energies (lab).

Here we discuss three energies; 230, 100, and 52 Mev.

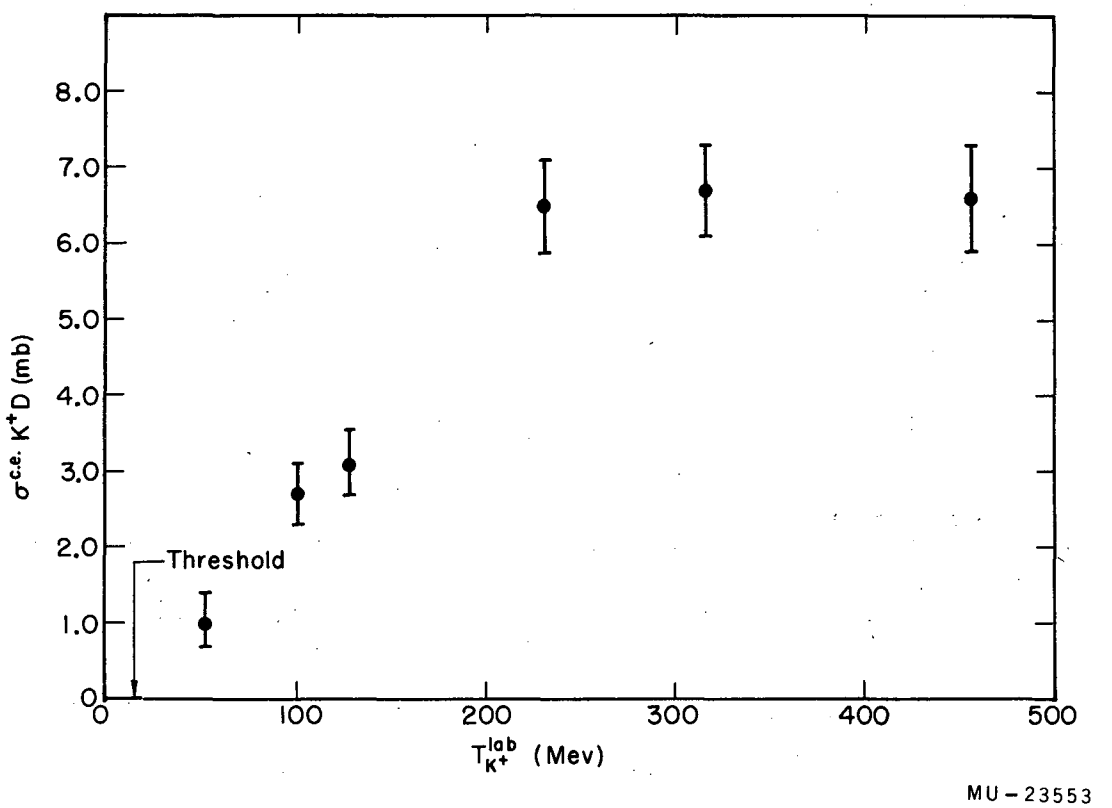

Fig. 4. The K^+-meson—deuteron charge-exchange total cross sections as a function of K^+-meson kinetic energies in the laboratory system.

Table II. Total K^+-d charge-exchange cross sections at six different energies between 52 and 456 Mev, along with the number of charge-exchange events with subsequent K_1^0 decay in each energy.

p (Mev/c)	T (Mev)	N_{ce}	σ^{ce} (mb)
230±40	52±17	13	$1.0^{+0.4}_{-0.3}$
330±23	100±13	46	2.7±0.4
377±18	127±11	65	3.1±0.4
530±15	230±11	161	6.5±0.6
642± 7	315±6	216	6.7±0.6
812± 6	456±5	196	6.6±0.7

230 Mev

The total cross section was obtained by two independent methods. One was by directly measuring the path length, the other by indirectly inferring the total path length by counting the number of effective τ decays.*

Out of 18,997 good frames, the tracks on a total of 1,931 frames were counted, which yielded 10,359 tracks. Every 10th frame was counted. If the 10th frame had neither tracks nor background, then the 15th was used. This gave a total of 1.02×10^5 K^+ tracks. The average passing track length was 20.0±0.4 cm, so we get $(2.13\pm0.10)\times10^6$ cm for the total path length. Corrections for tracks of decaying and interaction K^+, and also for ≈3% pion contamination, were included in this calculation.

*Effective τ decay is defined as any three-charged-particle decay mode of the K^+ meson. This includes the decay modes

$K^+ \rightarrow \pi^+ + \pi^+ + \pi^-$,
$K^+ \rightarrow \pi^+ + e^+ + e^-$,
$K^+ \rightarrow \pi^+ + e^+ + e^- + \pi^0$,
$K^+ \rightarrow \mu^+ + e^+ + e^- + \nu$,
$K^+ \rightarrow e^+ + e^+ + e^- + \nu$.

We used an effective τ branching ratio of 6.1±0.3%. Dr. William Chinowsky, now at Brookhaven National Laboratory, (private communication).

We observed 304 effective τ decays, which gives a total path length of $(1.96\pm0.24)\times10^6$ cm for the total path length. Since the observed number of events was 171 after correction for efficiency, and the density of deuterium is 0.0625 ± 0.0010 g/cm^3,* we obtain 6.5 ± 0.6 mb for the total cross section. The angular criteria previously mentioned were also strictly applied for effective τ's and passing K^+'s.

100 Mev

At this energy and at 52 Mev the angular criteria were not enforced, as explained before. Thus, just counting the passing K would not be sufficient to obtain the total path length, because not all tracks had the same length in the fiducial volume. We measured the length of every K^+—interacting, decaying, and passing—for every 10th frame. This way we obtained a total path length of 1.32×10^6 cm.

On the basis of 349 effective τ decays we get a total path length of $(1.38\pm0.10)\times10^6$ cm. This gives a total cross section of 2.7 ± 0.4 mb.

52 Mev

Almost half of the K^+ stopped in the chamber at this energy, rendering the effective-τ count of no use. The total path length was obtained by measuring every 10th frame, just as for the preceding energy. The error in the total cross section should take into account that the last 7 Mev is not available for the interaction, because the charge-exchange interaction is endothermic; but the large error due to the small number of events considerably dominates all other sources of error. From a total-path measurement of 1.2×10^6 cm, we obtained the charge-exchange total cross section of $1.0^{+0.4}_{-0.3}$ mb for an average interaction energy of 52 ± 17 Mev.

Differential Cross Sections

The scattering angle was calculated for both an initially stationary and an initially moving neutron. The initial momentum of a moving neutron was inferred from the spectator momentum. These two cases gave essentially identical angular distributions.

The angular distributions in the c.m. system for the moving-neutron case are plotted with $\Delta \cos\overline{\theta} = 0.4$ for lab kinetic energies of 100 and 127 Mev combined, as well as 230, 315, and 456 Mev, as shown in Fig. 5a. In Fig. 5b we show the same data with $\Delta \cos\overline{\theta} = 0.3$ to illustrate the effect of

*The density of deuterium was obtained by measuring the length of μ^+ mesons decaying from stopped π^+ mesons in the chamber. The density was found to be $(1.068\pm0.006)\times$ density of hydrogen (Mr. Ted Stubbs, University of California, Berkeley, private communication).

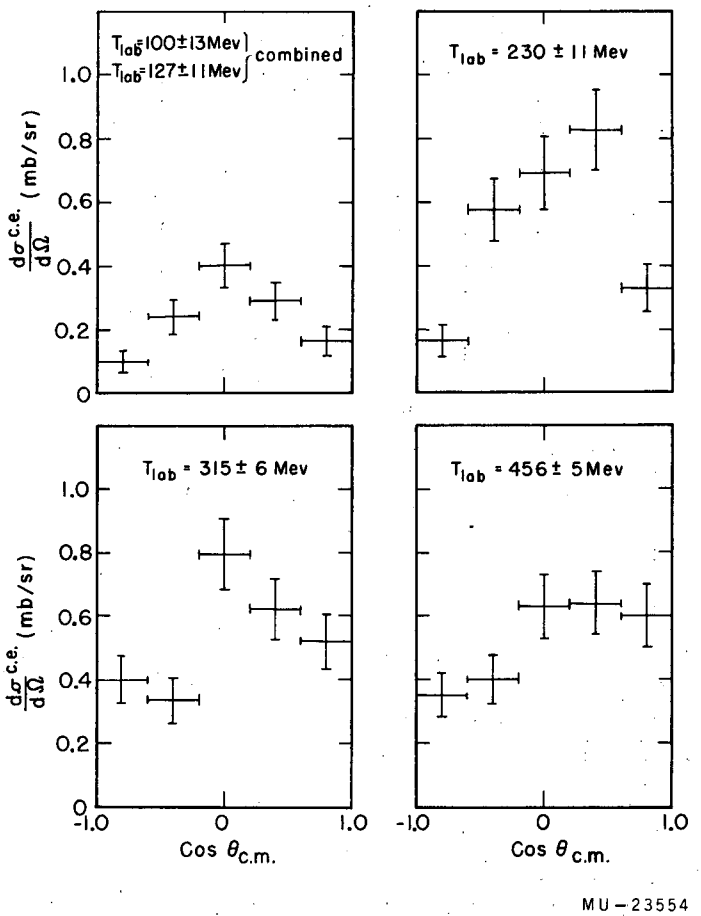

Fig. 5a. The K^+-meson—deuteron charge-exchange differential cross sections in the c.m. system of K^+ meson and moving neutron. The initial momentum of the neutron was inferred from the spectator momentum. Angular distributions are shown for lab kinetic energies of 100 and 127 Mev combined, as well as 230, 315, and 456 Mev; here $\Delta \cos \theta = 0.4$

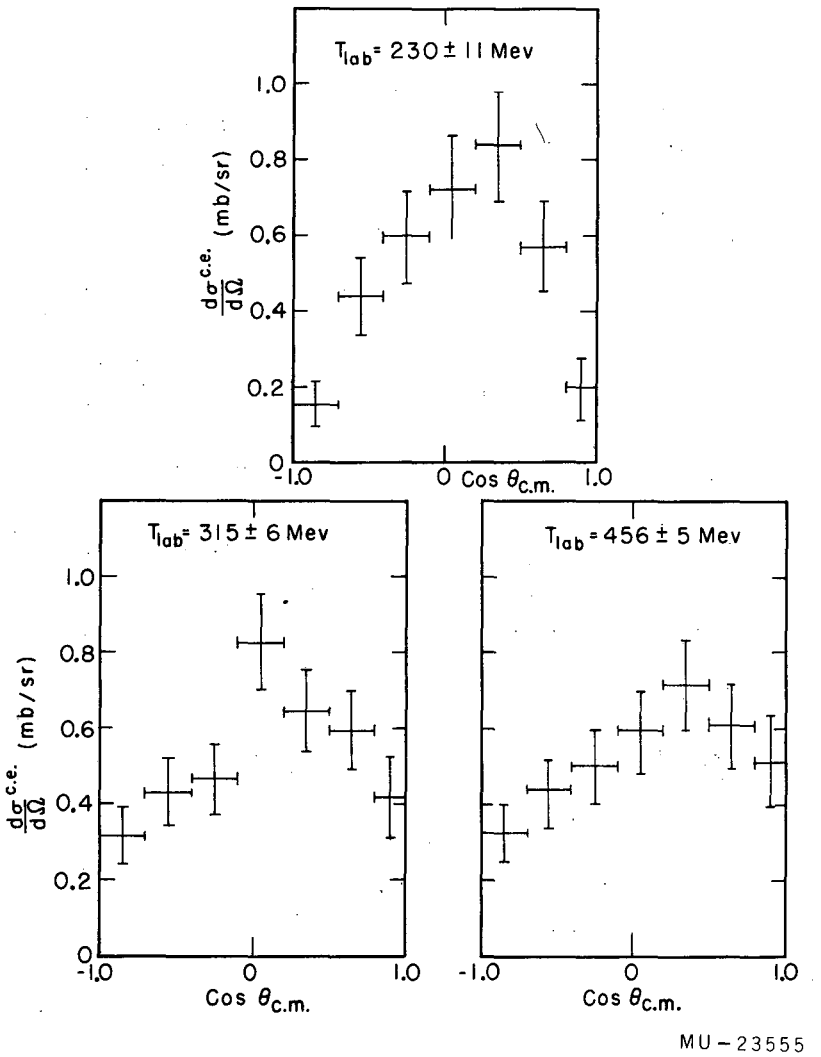

Fig. 5b. The K^+-meson—deuteron charge-exchange differential cross sections in the c.m. system of K^+ meson and moving neutron. The initial momentum of the neutron was inferred from the spectator momentum. Angular distributions are shown for lab kinetic energies of 230, 315, and 456 Mev; here $\Delta \cos \overline{\theta} = 0.3$. The lowest-energy data are omitted here because of their low statistics.

changing $\Delta \cos \bar{\theta}$. These two angular distributions, although apparently not very similar, give essentially the same set of phase shifts. Their minimum χ^2 are, however, not the same, as we shall see. In Fig. 5b the 100- and 127-Mev data are omitted because of statistics. In Fig. 6 the distributions of the same data are shown in the lab system.

IV. PHASE-SHIFT ANALYSIS

Impulse and Closure Approximations

Unlike the K^- meson, the K^+ meson interacts strongly with nucleons in only three processes. These three processes can be described by the Coulomb scattering amplitude M_c, and the two charge-independent scattering amplitudes M_0 and M_1, corresponding to total T spin 0 and 1, respectively. Here it is also assumed that $K^+ - K^0$ is a T-spin doublet:

Process	Amplitude
$K^+ + p \rightarrow K^+ + p$	$M_1 + M_c$
$K^+ + n \rightarrow K^+ + n$	$1/2\ (M_1 + M_0)$
$K^+ + n \rightarrow K^0 + p$	$1/2\ (M_1 - M_0)$.

The M_1 amplitude at the energies 175±25, 225±25, and 275±25 Mev was studied by Kycia, Kerth, and Baender,[7] and currently is also being studied in the energy range $15 \leq T \leq 450$ Mev.[5,8] Heretofore, little was known about M_0.[9] To learn about the M_0 amplitude we must look at the second or third interaction process. One could investigate M_0 by using a beam of K^0 mesons; however, K^0 beams of sufficient intensity are difficult to obtain. Furthermore, such events are not easily identified, and interpretation of them is difficult. It is customary to overcome these difficulties by using deuterons for targets. With such a target there are three possible processes,

$K^+ + d \rightarrow K^+ + d$ (elastic),

$K^+ + d \rightarrow K^+ + p + n$ (inelastic),

$K^+ + d \rightarrow K^0 + p + p$ (charge exchange).

Because of the difficulty in distinguishing events of the first two processes we have considered events of the last process only.

To extract information about $K^+ + n \rightarrow K^0 + p$ from $K^+ + d \rightarrow K^0 + p + p$, we use the impulse and closure approximations. The impulse approximation was proposed by Chew to reduce a three-body problem to a superposition of two-body problems.[10] Its main assumption is twofold:

(a) The collision time in high-energy scattering is very short in comparison with the period of the deuteron.

(b) The average distance between the two nucleons is much greater than the range of the K^+-meson—nucleon force.

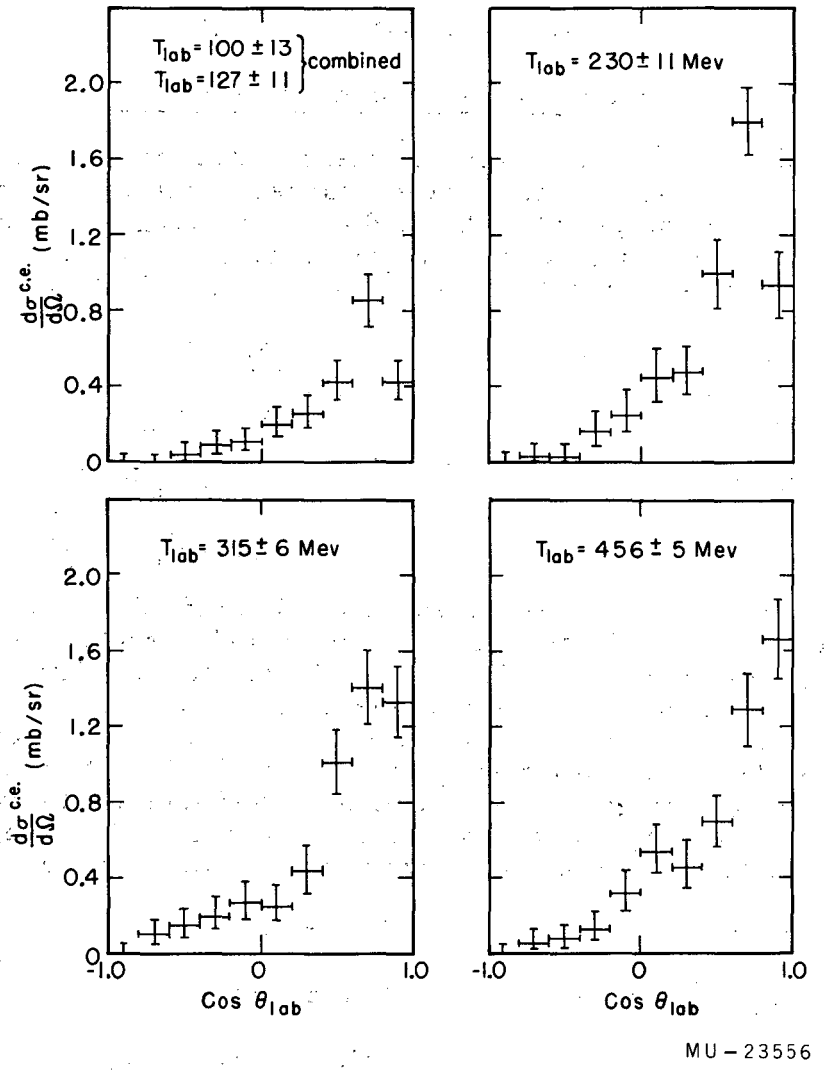

Fig. 6. The same data shown in Fig. 5 are shown in the laboratory system.

For the π-d system the impulse-approximation differential cross sections were expressed with phase shifts by Rockmore,[11] by using the pure scattering model of Fernbach, Green, and Watson[12] (to be referred to hereafter as FGW). The phase shifts were known from π^+-p and π^--p scattering experiments. The interactions of 85-Mev positive pions with deuterons were studied by Rogers and Lederman.[13] They showed that the impulse and closure approximations worked rather successfully for their case. By using the impulse and closure approximations, Ferreira[14] and, independently, Gourdin and Martin[15] derived the K^+-d differential cross section. Recently Ferreira[16] and Gourdin and Martin[17] independently took the final-state interactions of nucleons into account, assuming only an S wave in the M_0 amplitude.

We have experimentally tested the validity of the impulse approximation for our case in the following two ways. In the first test we compared the momentum distribution of the spectator protons with the nucleon momentum distribution in the deuteron. The impulse approximation assumes that the only effect of the spectator proton is the purely kinematical one of giving momentum to the interacting neutron during the decisive moment of collision. The spectator suddenly finds itself unbound and emerges from the collision with the momentum it possessed as a bound particle. Hence we expect the momentum distribution of the spectator proton to reflect the momentum distribution of a bound nucleon in the deuteron. We find indeed that the momentum distribution is in good agreement when compared with the Hulthén wave function for the nucleon momentum distribution in the deuteron. Because two protons emerge from an event there is some question which one is the spectator. However, it is reasonable to assume that the proton with the smaller momentum is the spectator. For the case in which both momenta are almost the same, the choice does not matter. Figure 7 compares the experimentally observed spectator distribution with the calculated Hulthén distribution. The smooth curve represents the Hulthén wave function in momentum space normalized to the same number of events. When the spectator was visible its momentum was measured directly(crosshatched in diagram); when it was not visible, its momentum was inferred from momentum conservation (not crosshatched in diagram). Agreement between the Hulthén distribution and the measured (and inferred) distribution is reasonably good. This suggests that the impulse approximation is good in our case, and that the charge-exchange scattering may be considered as a two-body problem. That it is indeed so can be demonstrated again by a second test. In a two-body problem, purely kinematical considerations tell us that for each scattering angle there is a unique momentum. Such would not be the case in three-body scattering events. Figure 8 shows a plot of experimentally observed K^0 momentum versus K^0 angle of emission in the laboratory system for our 530-Mev/c and 330-Mev/c events. This plot is to be compared with the smooth curve representing the expected kinematical relation for 530-Mev/c and 330-Mev/c mesons colliding with stationary nucleons. Again we have good agreement, but of course this test is not independent of the first test because of over-all momentum and energy conservation. The smooth curve should be regarded as the mean value of a band of curves that reflect the distribution in the momentum of the K^0 meson, because of the momentum distribution of the incoming beam and the effect of the momentum distribution of the neutron in the deuteron. The two tests indicate that there are relatively small amounts of both multiple and final proton-proton scattering.

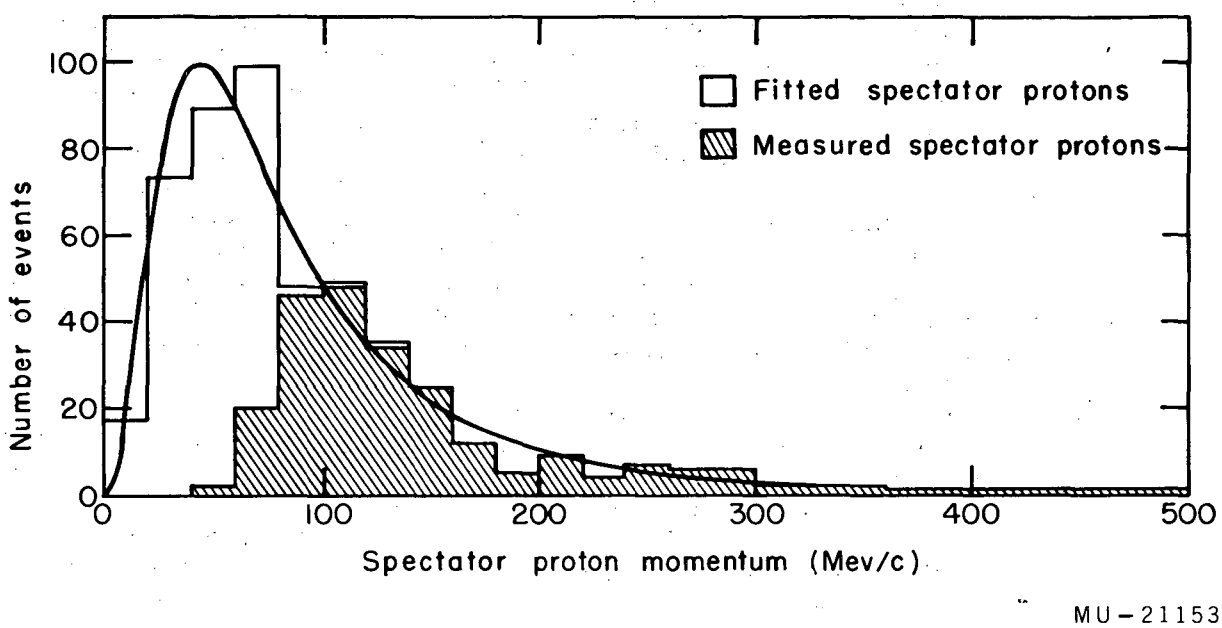

Fig. 7. Comparison of the experimentally observed spectator momentum distribution with the calculated Hulthén distribution. The smooth curve represents the Hulthén wave function in momentum space normalized to the same number of events. When the spectator was visible its momentum was measured directly (crosshatched in diagram), and when not visible, its momentum was inferred from momentum and energy conservation (no crosshatched in diagram).

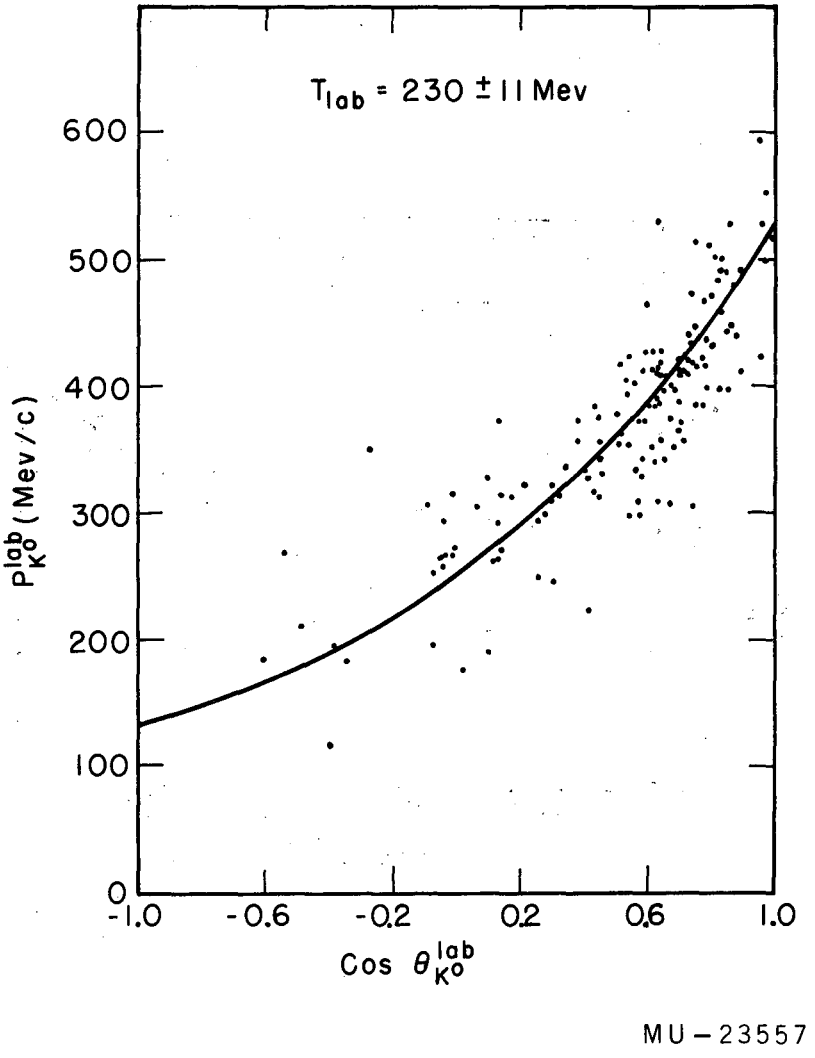

Fig. 8a. Experimentally observed K^0 momentum versus K^0 angle of emission (lab) for incident K^+ momentum of 530 Mev/c. The smooth curve represents the expected kinematical relation for a K^+ meson colliding with a nucleon.

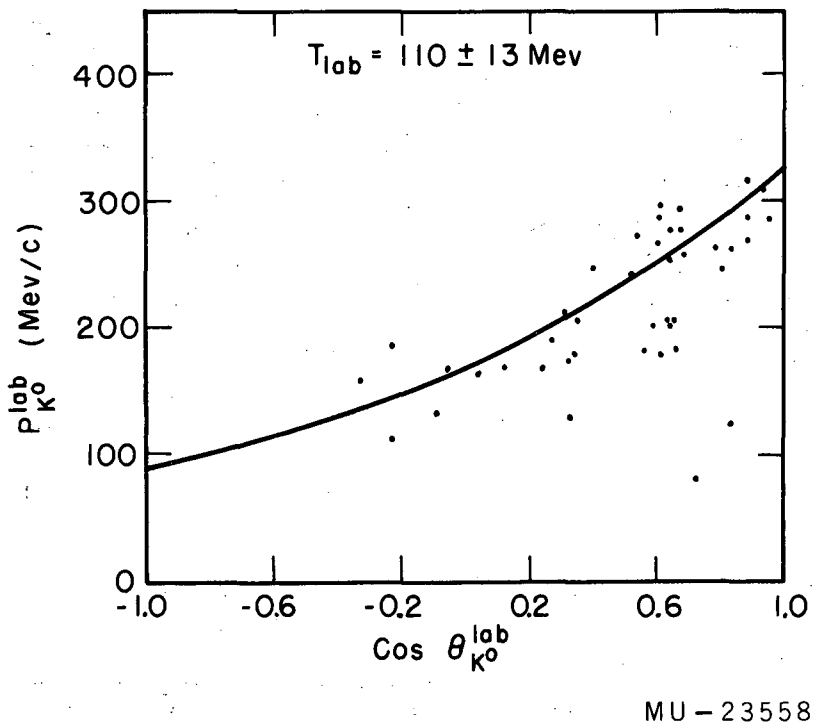

Fig. 8b. Experimentally observed K^0 momentum versus K^0 angle of emission (lab) for incident K^+ momentum of 330 Mev/c. The smooth curve represents the expected kinematical relation for a K^+ meson colliding with a nucleon.

Differential-Cross-Section Equation

For a free and stationary neutron target, the charge-exchange scattering matrix for either T-spin state is of the form

$$M(\bar{\theta}) = a(\bar{\theta}) + \vec{\sigma} \cdot \vec{n}\, b(\bar{\theta}),$$

where $\vec{n}$ is the unit vector perpendicular to the scattering plane, σ is the Pauli matrix, and $\bar{\theta}$ is the scattering angle in the K^+-n system (c.m.). After averaging over the initial spin state and summing over the final spin state, one finds that the differential cross section is

$$\frac{d\sigma}{d\bar{\Omega}} = |a(\bar{\theta})|^2 + |b(\bar{\theta})|^2 \qquad (4\text{-}1)$$

where

$$a = \frac{a_1 - a_0}{2}$$

$$b = \frac{b_1 - b_0}{2},$$

and the indices refer to T spin. For each T spin we have

$$a(\bar{\theta}) = \frac{1}{k} \sum_{\ell=0}^{\ell_{max}} \left[(\ell+1)\,\eta_\ell^{+} + \ell \eta_\ell^{-} \right] P_\ell^{0}(\bar{\theta})$$

and

$$b(\bar{\theta}) = \frac{i}{k} \sum_{\ell=1}^{\ell_{max}} (\eta_\ell^{+} - \eta_\ell^{-})\, P_\ell^{1}(\bar{\theta}) \qquad (4\text{-}2)$$

where $\eta = e^{i\delta} \sin\delta$, $\eta^{\pm}$ refers to $j = \ell \pm 1/2$, and k is the momentum in the K^+-n system (c.m.).

For the interaction $K^+ + d \rightarrow K^0 + p + p$, the impulse and closure approximations give*

$$\frac{d\sigma}{d\bar{\Omega}} = \left(|a|^2 + \frac{2}{3} |b|^2 \right)(1 - H_2) + \frac{1}{3} |b|^2 (1 + H_2), \qquad (4\text{-}3)$$

where

$$H_2(\bar{\theta}) = \frac{2(\alpha+\beta)\alpha\beta}{(\alpha-\beta)^2} \frac{1}{K} \left[\tan^{-1} \frac{K}{2\alpha} - 2 \tan^{-1} \frac{K}{\alpha+\beta} + \tan^{-1} \frac{K}{2\beta} \right],$$

$$K \approx 2k \sin \frac{\bar{\theta}}{2},$$

and

$$\beta = 7\alpha, \quad \alpha = 45.5 \text{ Mev}.$$

Here the Hulthén wave function was used for $\psi_D(r)$. In Fig. 9 we show $H_2(\bar{\theta})$ as a function of $\bar{\theta}$ for four different momenta k.

In the derivation of Eq. (4-3), as shown in Appendix D, the generalized Pauli principle for two outgoing protons is taken into account, but nowhere in this derivation does one consider corrections due to the final proton-proton interactions, multiple scattering, and K^+ - K^0 mass difference. Ferreira has pointed out that, in the energy region we are working on, the mass difference and multiple-scattering correction may be very small, except perhaps for small-angle scattering.[16] Corrections due to the final proton-proton interaction, however, may not be small. This correction term has been evaluated by several authors.[16,17]

In the phase-shift analysis we would like to have $\int_{\cos\bar{\theta}_i}^{\cos\bar{\theta}_j} \frac{d\sigma}{d\bar{\Omega}}\, d\bar{\Omega}$, which may be evaluated by simply integrating Eq. (4-3). The integrated results are shown in Appendix D, Eq. (D-12).

Phase-Shift Results

In this section we present several sets of phase-shift solutions and their errors, which we obtained from the phase-shift search and error programs. T = 1 phase shifts were assumed to be pure S wave. This knowledge comes from the elastic K^+-p scattering experiments.[5,7,8] In our analysis only T = 0 phase shifts were considered as unknowns. We discuss the fits to our data of the S, SP, and SPD waves for T = 0. We did not consider any higher partial waves because of the limitation of our statistics. In our analysis we took into account the following consideration, as was discussed before: Although at present it is difficult, if not impossible, to calculate quantitatively the correction terms due to the final proton-proton interactions, multiple scattering, and the mass difference, it is not difficult to show qualitatively that these correction terms may be small—except perhaps in the forward angular region.[19]

The phase-shift analysis was carried out both with and without the forward angular data. We found in both cases that, within the errors, the solutions common to the two cases were identical, although the minimum χ^2's we obtained for each case were not identical.

Errors in the T = 0 phase shifts come from several sources:
(a) Phase-shift errors that reflect experimental errors.

---

* $\frac{d\sigma^{ce}}{d\Omega}$ (lab) was given by Ferreira.[14] Here his equation is transformed to the c.m. of the K^+-n system. A discussion and derivation of Eq. (4-3) are in Appendix D.

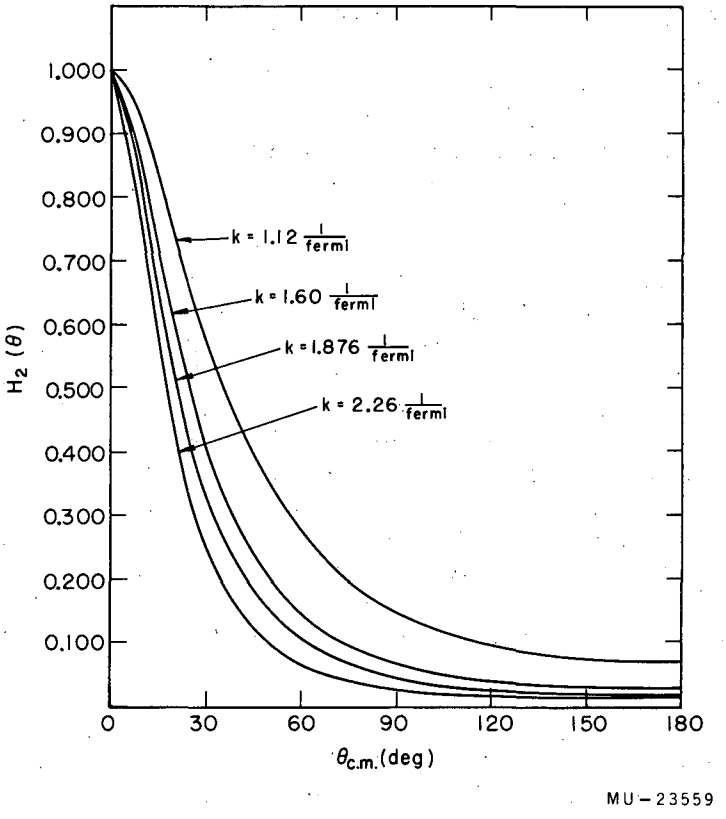

Fig. 9. Plot of $H_2(\theta)$ as a function of θ, c.m. angle, for c.m. momenta of 1.12, 1.60, 1.876, and 2.26 (1/fermi).

(b) Errors in S, P, and possibly D waves due to the errors in T = 1 phase shifts. (c) Errors reflected in the phase shifts due to the neglect of higher partial waves. (d) Errors due to spread in c.m. energy because the initial neutron is not at rest. (e) Errors due to the neglect of pion production at 812 Mev/c. (f) Errors due to the theoretical uncertainties.

We have no way of estimating errors due to (c) and (f). Errors due to (b) were calculated and found to be less than approx 3 deg. Errors due to (d) and (e) were again estimated and found to be negligible. The errors due to (a), calculated by the error program, were believed to be the largest in our case.

Phase shifts were obtained by using the phase-shift search program (see Appendix B for the meaning of n, ϵ, and M). For the large values of n and ϵ, i.e., n = 4, ϵ = 2.3 deg, the machine converges to the vicinity of minimum χ^2 rather rapidly from the randomly selected points. For the SP-waves fit it took an average of 15 to 20 sec to reach the vicinity of the minimum. For each set of data we tried some 200 to 300 random numbers. From this output we found how many different sets of phase shifts existed in each set of data. The phase shift that gave a minimum χ^2 in each set of solutions was selected and fed into the machine again to converge from this phase shift to reach the minimum with very stringent conditions, n = 1, ϵ = 0.23 deg. In this way we believe the minimum was reached to within 0.5 deg. We need to know the minimum point well in order to employ the error-matrix analysis.

Using the minimum just mentioned, we calculated the error matrices for each case with $\Delta\delta$ = 0.02, 0.03, 0.04, 0.06, and 0.08 radian (see Appendix C for the meaning of $\Delta\delta$). We examined the error matrix to see if the errors changed rapidly as a function of $\Delta\delta$. It was found that in many cases the errors with $\Delta\delta$ = 0.08 radian were substantially different from those with $\Delta\delta$ = 0.02, 0.03, 0.04, and 0.06 radian. The errors found by using $\Delta\delta$ = 0.02, 0.03, and 0.04 radian were substantially the same in most cases. We also found that $\Delta\delta$ = 0.03 radian corresponded to $\Delta M \lesssim 1$. The errors quoted below are, accordingly, for the error matrix calculated by using $\Delta\delta$ = 0.03 radian. Errors were also calculated by use of the direct method (see Appendix C), and were in excellent agreement with those from the error-matrix analysis for the SP-waves case. For the SPD case the direct method became too lengthy and inefficient, therefore no check was made.

S-wave fit

No attempt was made to fit the data with T = 0 S wave alone, because the differential cross section clearly indicated the presence of the higher-angular-momentum states (see Appendix E).

SP-waves fit

At each energy the data were split into a number of angular intervals in three different ways. Because there are three phase shifts to be determined, we need four or more angular intervals to give one or more constraints. The three ways of splitting up the region of cos θ were as follows: ( )

(a) (-1.0, -0.6), (-0.6, -0.2), (-0.2, 0.2), and (0.2, 0.6)—(see Fig. 5a); (b) (-1.0, -0.7), (-0.7, -0.4), (-0.4, -0.1), (-0.1, 0.2), (0.2, 0.5), and (0.5, 0.8)—(see Fig. 5b), and (c) four angular intervals between $\cos\bar{\theta} = -1.0$ and $\cos\bar{\theta} = 1.0$ chosen to have roughly the same number of events in each interval. We found that each set of data gave two sets of solutions, A and B (see Table III), for every energy—each set having two additional solutions because of the Fermi-Yang ambiguity. We do not, however, have the Minami ambiguity because we fixed the $T = 1$ phase shift to be pure S wave. We found the same set of phase shifts independent of the manner in which we split our data, but different distributions did not give the same minimum χ^2, although their solutions were identical within errors.

Two sets of solutions differed in the magnitude of S wave; small S-wave solutions gave 4 to 6 mb and large S-wave solutions 20 to 30 mb for the K^+-n total elastic cross section. In Table III we list all the phase-shift solutions with errors, the calculated K^+-d total elastic and inelastic cross sections, and the confidence limit of the phase shifts.

From the known total cross sections of the K^+-d reaction at 330 and 800 Mev/c, and from the requirement of smooth variations in phase shifts and in the K^+-d total elastic and inelastic cross sections with energies, we find we can discard the phase shifts with large S wave, the set B. This point is discussed in detail in Appendix A. The final result is that we are left at each energy with the two Fermi-Yang solutions of the set A, one of which may be eliminated in the future by studying the polarization of the recoil proton. In Fig. 10 we show the energy dependence of phase shifts of the set A. As can be seen in Fig. 10, the $T = 0$ phase shift shows a smooth variation with momentum in the K^+-n c.m. system.

In Fig. 11 we show the experimental cross sections, and the cross sections calculated by the set A. The set of data that gave the smallest χ^2 is shown in the lower diagram. The dotted curves show the free-neutron charge-exchange cross sections. The dotted experimental data were not used for the phase-shift analysis. In the upper diagram the differential cross section for K^+-n elastic cross sections is shown.

One can see both in Fig. 11 and in the confidence limits given in Table III that the SP fit is reasonably good when we consider all energies and the theoretical uncertainties and others that we have already discussed.

SPD-waves fit

Here we have five phase shifts to be determined. The data were therefore split into six intervals, giving one constraint. The data splitting was done by two methods, so that forward data was included one way but was not included the other way. The one without forward data was split into intervals of $\cos\bar{\theta}$ from $\cos\bar{\theta} = -1.0$ to 0.8 (Fig. 5b). These data gave us three sets of phase shifts; each set usually contains two solutions roughly corresponding to the Fermi-Yang ambiguity. (With D wave included, there is no rigorous Fermi-Yang ambiguity.) The other way of splitting the data, which included the entire angular interval, gave us the same number of sets of solutions; these solutions were identical, within errors, to the three sets of solutions of the other distribution.

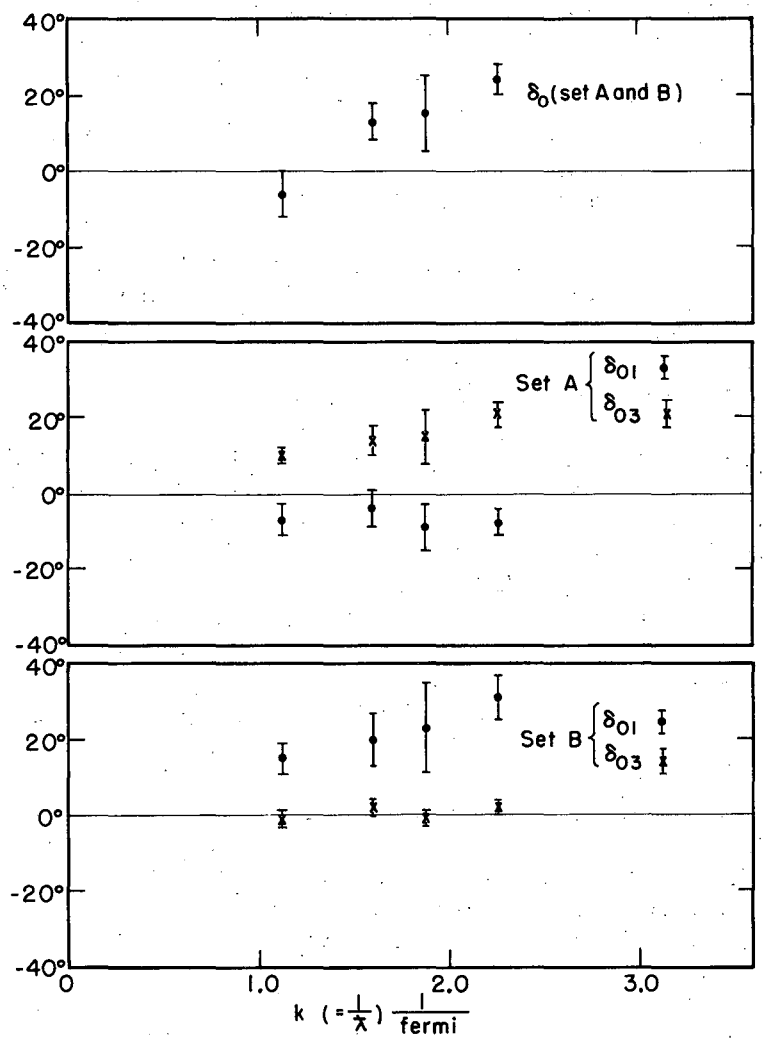

Fig. 10. Energy dependence of phase shifts of the set A.

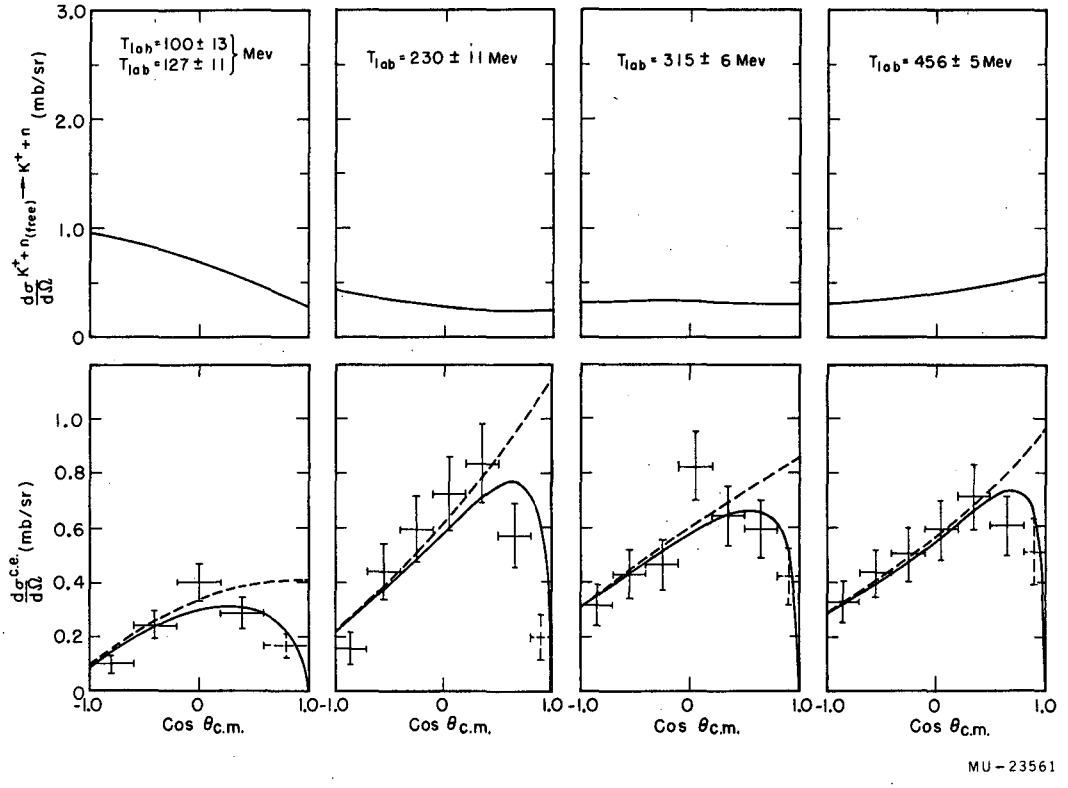

Fig. 11. The experimental differential cross sections, and those calculated by the phase shift set A. In the lower diagrams we indicate calculated charge-exchange differential cross sections on deuterons by solid curves, and those on free neutrons by dotted curves. In the upper diagrams we show the K^+-neutron elastic differential cross sections.

Table III. Phase-shift solutions with errors for sets A and B. The sets A and B are small and large S-wave solutions in the SP fit. Errors quoted are $(G^{-1})_{ii}$ deg. (In Table IV we show the error matrices of set A.)

Set A

Numbers[a]	T (Mev)	p (Mev/c)	T = 1 $S_{1/2}(\delta_1)$ (deg)	T = 0 $S_{1/2}(\delta_0)$ (deg)	T = 0 $P_{1/2}(\delta_{01})$ (deg)	T = 0 $P_{3/2}(\delta_{03})$ (deg)	Confidence limit (%)	σ^{E+I}_{calc} (mb)	σ^{E+I}_{exp} (mb)
1	113	356	-23	-6±6	-7±4	10±2	4	27	21±5
2					15±4	-1±2			
3	230	530	-34	13±5	-4±5	14±4	2	21	
4					20±7	2±2			
5	313	642	-41	15±10	-9±7	15±7	16	20	
6					23±12	-1±2			
7	456	812[d]	-50	24±4	-8±3	21±3	70	19	20±2
8					31±6	2±2			

[a] This number is for correlation with the error matrix in Table IV.

[b] Here σ^{E+I} is calculated with a cutoff angle of $\cos\theta_{lab} = 0.94$. Errors in calculated σ^{E+I} reflected from errors in phase shifts are small (≈ 3 deg) and are not quoted. See Appendix A.

[c] See Appendix A.

[d] Additional large positive S-wave solutions exist for this energy:

δ_0	δ_{01}	δ_{03}
55 deg	25 deg	-3.5 deg
	-9 deg	20 deg

We exclude this set because of the assumption of smooth variation of S-wave phase shift with energy.

UCRL-9691

Table III (continued)

T (Mev)	p (Mev/c)	T = 1 $S_{1/2}(\delta_1)$ (deg)	T = 0 $S_{1/2}(\delta_0)$ (deg)	T = 0 $P_{1/2}(\delta_{01})$ (deg)	T = 0 $P_{3/2}(\delta_{03})$ (deg)	Confidence limit (%)	E+I σ_{calc} (mb)	E+I σ_{exp} (mb)
113	356	-23	-33±8	-18±6	4±4	20	47	21±5
				13±3	-10±4			
230	530	-34	-68±12	-26±13	15±10	50	45	
				29±11	-12±9			
313	642	-41	-54±20	-57±15	10±8	20	40	
				48±15	-19±8			
456	812	-50	-76±12	-75±30	2±10	70	35	20±2
				59±30	-20±10			

Table IV. Error matrices for the set A in the SP fit. The matrix elements are in $(\text{deg})^2$.

		δ_0	δ_{01}	δ_{03}
(1)	δ_0	31	20	-7
	δ_{01}		16	-3
	δ_{03}			4
(2)	δ_0	38	-24	12
	δ_{01}		19	-6
	δ_{03}			6
(3)	δ_0	27	19	-15
	δ_{01}		23	-14
	δ_{03}			15
(4)	δ_0	28	-29	6
	δ_{01}		46	-8
	δ_{03}			4
		δ_0	δ_{01}	δ_{03}
(5)	δ_{01}	101	48	-65
	δ_{01}		33	-33
	δ_{03}			50
(6)	δ_0	98	-104	1
	δ_{01}		131	0
	δ_{03}			4

Table IV (continued)

		δ_0	δ_{01}	δ_{03}
(7)	δ_0	15	-2	-2
	δ_{01}		7	-1
	δ_{03}			7
(8)	δ_0	18	20	-8
	δ_{01}		33	-1
	δ_{03}			4

Two sets, A' and B', of the three we obtained were identifiable with the sets A and B in the SP fit with small D waves added (see Table V). In addition a new set of phase shifts, set C', was obtained (see Table V). Set B' gave a large K^+-d total cross section, as set B had done previously, and was accordingly eliminated. In Table V we list the two sets A' and C', the calculated K^+-d total elastic and inelastic cross sections (σ^{E+I}), and the confidence limit of the phase shifts.

In Fig. 12 we show the experimental K^+-d charge-exchange differential cross sections. The cross sections calculated by set C' are in the lower diagram. The meanings of the dotted curves and data are the same as those of Fig. 11. Set A' was not plotted because it differs little from set C' in the lower diagrams. In the upper diagrams, however, where the K^+-n elastic differential cross sections are shown, the sets A' and C' are markedly different. The K^+-n elastic differential cross sections of set C' are shown in Fig. 12; those of set A' are almost the same as those of set A (shown in Fig. 11). In principle, the set A' or C' may be eliminated by a measurement of the K^+-n elastic differential cross section. An error-matrix analysis was carried out with sets A' and C'. We found that errors were quite large, and we concluded that our data were not statistically accurate enough to determine the five parameters involved here.

In Fig. 13 we show the differential cross sections (lab) calculated with set A at combined 330 and 377 Mev/c, and the set C' for the other momenta.

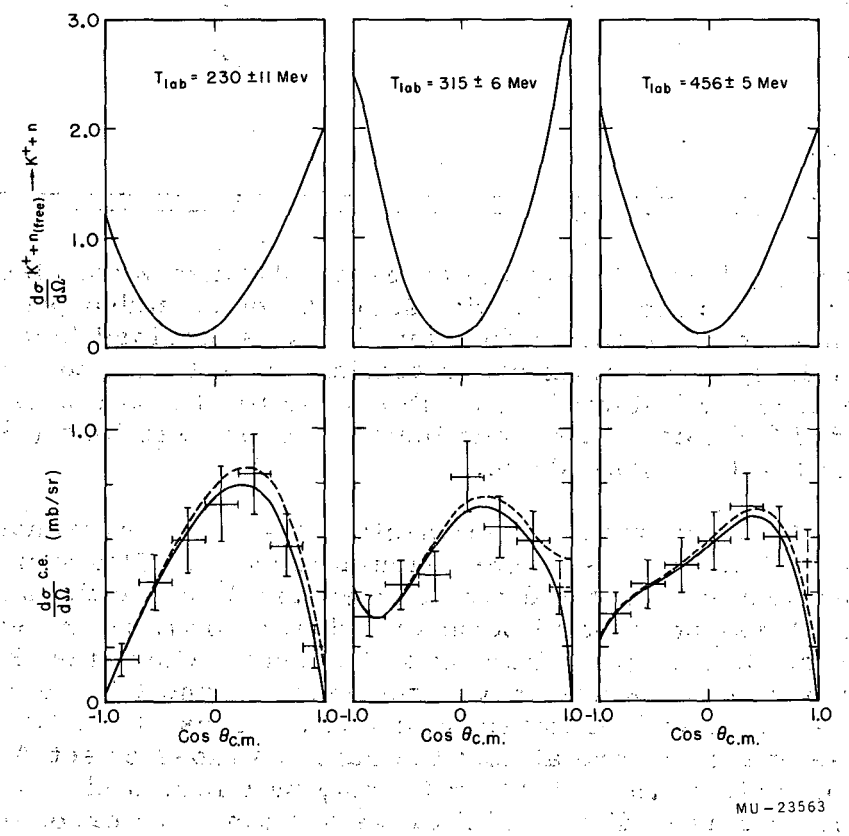

Fig. 12. The experimental differential cross sections, and those calculated by the phase-shift set C'. In the lower diagrams we indicate calculated charge-exchange differential cross sections on deuterons by solid curves, and those on free neutrons by dotted curves. In the upper diagrams we show the K^+-meson—neutron elastic differential cross sections.

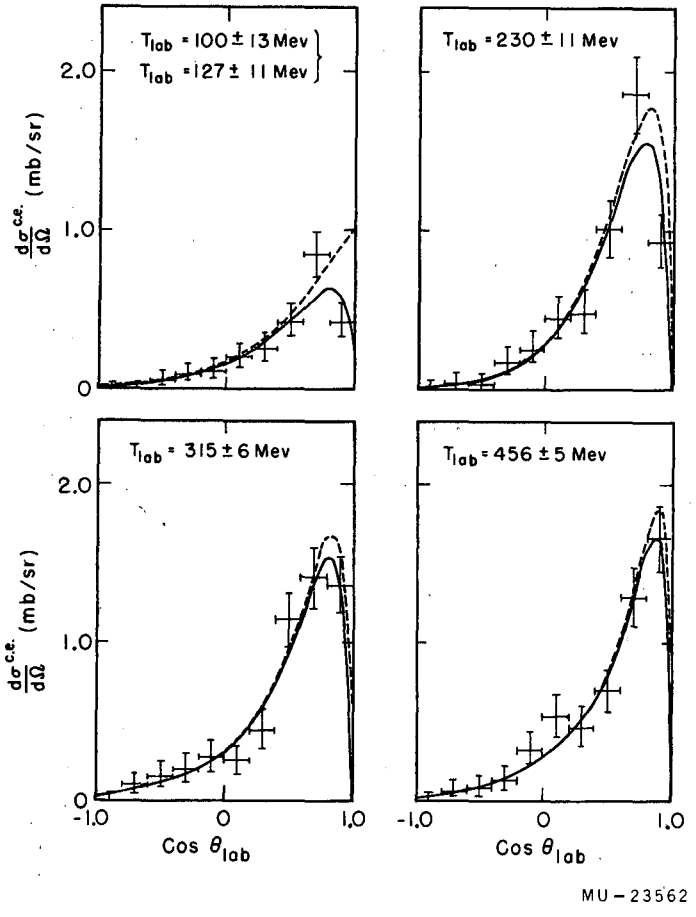

Fig. 13. The experimental charge-exchange differential cross sections (lab), those calculated by the set A for the combined 100 and 127 Mev, and those calculated by the set C' for the rest of the energies. We indicate calculated charge-exchange differential cross sections on deuterons by solid curves, and those on free neutrons by dotted curves.

Table V. Phase-shift solutions from the SPD-waves fit, for sets A' and C'

Set A'

T (Mev)	p (Mev/c)	T=1 $S_{1/2}(\delta_1)$ (deg)	T=0 $S_{1/2}(\delta_0)$ (deg)	$P_{1/2}(\delta_{01})$ (deg)	$P_{3/2}(\delta_{03})$ (deg)	$D_{3/2}(\Delta_{03})$ (deg)	$D_{5/2}(\Delta_{05})$ (deg)	Confidence limit (%)	σ^{E+I} calc (mb)	σ^{E+I} exp (mb)
230	530	-34	9	-8	13	-5	-3	30	21	
			11	17	2	-6	-2	30	21	
313	642	-41	14	-10	14	-3	-1	8	20	
			13	24	0	-2	-2	8	21	
456	812	-50	28	-11	16	-1	0	70	18	20±2
			22	29	1	-2	-1	70	18	20±2

Set C'

T (Mev)	p (Mev/c)	T=1 $S_{1/2}(\delta_1)$ (deg)	T=0 $S_{1/2}(\delta_0)$ (deg)	$P_{1/2}(\delta_{01})$ (deg)	$P_{3/2}(\delta_{03})$ (deg)	$D_{3/2}(\Delta_{03})$ (deg)	$D_{5/2}(\Delta_{05})$ (deg)	Confidence limit (%)	σ^{E+I} calc (mb)	σ^{E+I} exp (mb)
230	530	-34	-4	10	-9	5	-16	45	24	
			-5	-15	3	-22	0	40	25	
313	642	-41	-16	7	-5	5	-26	8	26	
			-11	-5	-6	-29	0	8	25	
456	812	-50	-15	10	-2	12	-27	75	18	20±2
			-6	-33	6	-20	5	80	21	20±2

V. DISCUSSIONS OF RESULTS

The total cross sections of K^+-meson charge-exchange scattering on deuterons at six different energies from the threshold up to 456 Mev were obtained. The total cross section rises rapidly from the threshold up to $\approx$ 230 Mev and is constant from $\approx$ 230 Mev to $\approx$ 456 at a value of $\approx$ 6.5 mb. At four different energies the differential cross sections were also obtained. Our data confirmed the existence of appreciable P waves in the T = 0 amplitude for K^+ kinetic energy as low as 113 Mev (lab).

A phase-shift analysis was performed for each energy by use of the conventional least-squares fit. Phase-shift errors were calculated by the usual error-matrix analysis, and were checked by the direct method.

Recent experiments on K^+-p elastic differential cross sections are consistent with the T = 1 state's being dominantly pure S wave, $P_{1/2}$ wave, or a mixture of $P_{1/2}$ and $P_{3/2}$ waves in the K^+-meson kinetic energy region of our interest. The constant value of the K^+-p total cross section as a function of energy above 100 Mev suggests that the T = 1 state is dominantly S wave. Throughout our analysis the T = 1 state is assumed to be pure S wave. If the T = 1 state turned out to be dominatly the $P_{1/2}$ state, then the T = 0 state would be the Minami transformation of our results. If the T = 1 state turned out to be a mixture of $P_{1/2}$ and $P_{3/2}$ states, the T = 0 phase shifts would have to be calculated again.

We searched for the SP-waves fit for the T = 0 amplitude and obtained two sets of phase shifts that were identical for the several different ways we split the angular intervals. In addition each set has two different solutions corresponding to the Fermi-Yang ambiguity. The two different sets gave considerably different K^+-d total cross sections. On this basis we were able to discard one of the two sets. The remaining set fits the data reasonably well when all the energies and the theoretical difficulties of the analysis are considered. If we assume that the T = 0 amplitude is S and P waves only, we are left with the unique set A, shown in Table III. This set of solutions shows that P wave is definitely present in the T = 0 amplitude. This set also shows that the sign of the S-wave phase shift changes from negative to positive as the energy of the K^+ meson increases.

Set A shows a smooth variation with the c.m. momentum of the K^+ meson, as shown in Fig. 10. As can be seen from Fig. 10, the P-wave phase shift definitely cannot be considered as dependent on the cubic power of the c.m. momentum of the K^+ meson.

There is, however, no reason to believe that there are only S and P waves in the T = 0 amplitude. At present there is no way of knowing the upper limit on the partial waves, and one is limited to a small number of partial waves because of the limitations of statistics. Classical arguments can be employed to justify taking only a few angular momentum states into consideration in the low-energy region.

It is well known that consideration of an additional angular-momentum state not only increases the error in the individual phase shifts, but also creates an additional set of phase shifts. In our analysis we considered the SPD fit, except for the 100- and 127-Mev data.

In the SPD fit we obtained three sets of phase shifts--sets A', B', and C'. Sets A' and B' were identifiable with sets A and B in the SP fit with small D waves added. In addition, a new set of phase shifts, the set C', was obtained. Set B' gave as large a K^+-d total cross section as set B did, and was accordingly eliminated. Both sets A' and C' gave a K^+-d total cross section consistent with the known data, but their differential cross sections for the K^+-n elastic scattering were quite different. Set A' or C' may be eliminated in the future by a measurement of the K^+-n elastic differential cross section.

An error-matrix analysis was carried out for sets A' and C'. We found that the errors in the SPD fit were quite large, and we concluded that the present data are not statistically accurate enough to determine the five parameters involved here.

In our analysis the elementary differential cross section was expanded into the partial waves with the aid of the impulse and closure approximations. Justification for using these approximations comes primarily from the experimental evidence we discussed earlier. A phase-shift analysis was carried out both with and without the data in the forward angular region. We found that the results did not depend on whether or not the forward angular data were included. It may be that the Pauli principle dominates over the multiparticle and mass-difference effects in the forward region. Then the multiparticle and mass-difference effects would be too small to be detected by our limited statistics. In the future, with much better statistics, a more serious study of the correction terms will perhaps be necessary to determine the phase shift more accurately.

Several authors have attempted to calculate the scattering length and effective range of K^+-N interactions by the double-dispersion theory.[20, 21] Because of the very preliminary nature of such theories, we make no attempt to discuss how well they fit out data.

ACKNOWLEDGMENTS

I would like to express by sincere appreciation to Professor Gerson Goldhaber for his guidance and encouragement during this work and through several years of graduate study.

I am grateful to Dr. Sulamith Goldhaber for her advice during many phases of my graduate work.

I am indebted to Dr. William Chinowsky and Dr. Hugh Bradner for their advice during this work.

This work was performed in cooperation with a group from the University of California, Los Angeles. Gratitude is due Professor William Slater, Professor Donald Stork, and Professor Harold K. Ticho. In particular, special gratitude is due Professor Ticho for his advice during this work.

Many thanks are due to Mr. Thomas O'Halloran and Mr. Theodore Stubbs as co-workers on many projects for the past several years, to Mr. Donald Itzel and Mrs. Marjory Simmons for the IBM programming, to Mr. Kirmach Natani for the operation of the IBM machines, and to Mr. Martial Thiebaux for many discussions.

Professor Luis Alvarez directed the IBM programming of the PANG and KICK programs, and the building of the 15-inch bubble chamber.

The Bevatron and bubble chamber crews were extremely helpful during the experimental run.

Finally, no list of acknowledgments would be complete without mentioning people responsible for scanning and measurements. I am grateful to Mr. George Baker, Mr. Michael Guinan, Mrs. Lora Langner, Mrs. Frances Simon, Miss Joan Dyleski, Mrs. Jean Firby, Mr. Joseph Gutierrez, Mrs. Joann Kendall, Mr. John Korver, Mrs. Rosanne Levitt, Miss Harriett Rice, Mr. Bryce Sheldon, Mr. Lawrence Stern, Mr. George Swaney, and Mr. David Teselle.

This work was done under the auspices of the U. S. Atomic Energy Commission.

APPENDICES

A. Measurement and Calculation of the Total Elastic and Inelastic Cross Sections

Because of the rather large difference between the total elastic and inelastic cross sections given by the two different types of phase-shift sets--i.e., large and small S wave in both SP and SPD fits--even a crude estimate of the total elastic and inelastic cross sections is desirable to eliminate one or the other. We define $K^+ + d \rightarrow K^+ + d$ as elastic and $K^+ + d \rightarrow K^+ + p + n$ as inelastic.

A total elastic and inelastic cross section at 300 Mev/c has been measured and found to be 21±5 mb with a cutoff angle of 20 deg (lab). The method for finding this cross section is discussed below. The K^+-d total cross section has been measured at 800 Mev/c by Kerth et al., and found to be 26.3±0.7 mb.* This gives $\sigma^{E+I} = 19.7 \pm 2$ mb. The sets B and B' at 330 and 810 Mev/c are definitely ruled out when one compares the measured and calculated σ^{E+I}. The assumption of a smooth variation of phase shifts and total cross sections with energy is sufficient to rule out the sets B and B' of the two intermediate energies.

Measurement of σ^{E+I} at 330 Mev/c

At 330 Mev/c the momentum of K^+ mesons is low enough so that it is not difficult to tell the K^+ from the lighter mesons or protons by the curvature and ionization of tracks in the chamber. It is also not difficult to find out, by the change in the ionization and curvature at the vertex, whether or not the incoming K^+ meson decays or interacts. The same is not true, however, for the K^+ meson at 530 Mev/c Thus it is possible to obtain the σ^{E+I} at 330 Mev/c by scan-table measurements without going through a complete analysis.

In the determination of the total cross section it is imperative to know which one of the outgoing particles is the K^+ meson for small scattering angles. One can then introduce the cutoff angle to correct for the Coulomb scattering. For a small scattering angle the momentum transfer is small, thus the recoil often comes to rest. For scattering in the backward hemisphere the K^+ meson is easy to identify because the track is very dark and it often decays in the chamber.

Upon rescanning approximately 60% of the pictures we found the distribution to be as summarized:

---

*The author would like to thank Dr. Leroy Kerth and Mr. Carl M. Noble for providing him with the unpublished data.

Elastic and inelastic scattering

Projected angle (deg)	20 to 40	40 to 90	90 to 180
Number of events	184	223	130

Charge exchange

112 events

The numbers quoted here are already corrected for detection efficiency. The number of events from 0 to 20 deg is not quoted because of uncertainty in efficiency. A correction for the variation of the camera angle for different positions in the bubble chamber can be shown to be negligible for our case.

In about 10% of the events we could not tell which track was the K^+ meson. In such cases the prong with the smaller angle was assumed to be the K^+. Errors due to this assumption were incorporated into the final calculation of the total cross section.

The total elastic and inelastic cross sections in the backward hemisphere can be calculated directly. Here we make use of the total path length we obtained for the charge-exchange case. We obtain

$$\sigma_{exp}^{E+I} (\geq 90 \text{ deg}) = 4.0 \pm 0.7 \text{ mb},$$

$$\sigma_{cal}^{E+I} (\geq 90 \text{ deg, small S wave}) = 4.0 \pm 0.4 \text{ mb},$$

and

$$\sigma_{cal}^{E+I} (\geq 90 \text{ deg, large S wave}) = 5.8 \pm 0.3 \text{ mb}.$$

The backward-hemisphere data alone favor the small S-wave solution, but are not sufficient to eliminate the large S-wave solution. When the cutoff angle is 20 deg,

$$\sigma_{cal}^{E+I} (\geq 20 \text{ deg, small S wave}) = 27 \pm 3 \text{ mb}$$

and

$$\sigma_{cal}^{E+I} (\geq 20 \text{ deg, large S wave}) = 46 \pm 3 \text{ mb}.$$

A crude estimate of the total cross section with cutoff angle of 20 deg would decide which set of phase shifts is consistent with the data.

In order to calculate $\sigma_{exp}^{E+I} (\geq 20 \text{ deg})$, we need to know the number of events (ΔN) with a scattering angle greater than 20 deg but with a projected angle less than 20 deg. We have

$$\Delta N(\text{in mb}) = 2\pi \int_{\theta=20^\circ}^{90^\circ} f(\theta) \frac{d\sigma}{d(\cos\theta)} \, d(\cos\theta),$$

where

$$f(\theta) = 1 - \frac{2}{\pi} \cos^{-1} \frac{\tan 20^\circ}{\tan \theta} .$$

Here $f(\theta)$ is the portion of events between the projected angle of 0 to 20 deg with a scattering angle θ.

$$\left\langle \frac{d\sigma^{E+I}}{d\Omega} \right\rangle_{av} \quad (\theta = 20 \text{ deg to } 40 \text{ deg}) \quad \text{and} \left\langle \frac{d\sigma^{E+I}}{d\Omega} \right\rangle_{av} \quad (\theta = 40 \text{ deg to } 90 \text{ deg})$$

can be obtained from the known number of events between projected angles of 20 to 40 deg and 40 to 90 deg. Using these average differential cross sections, one obtains ΔN. The result of this calculation is $\Delta N = 130 \pm 50$ events, which gives σ^{E+I} ($\geq$ 20 deg) = 21±5 mb.

Calculation of Total Elastic and Inelastic Cross Section

Total cross sections are calculated with the phase shifts that we obtained in Section III. The differential cross sections for elastic, elastic plus inelastic, and charge-exchange scattering were given in terms of phase shifts by Ferreira,[14] in a calculation patterned after FGW. In Appendix D we discuss the necessary steps to get the charge-exchange differential cross section. Unlike the charge-exchange scattering, for the elastic plus inelastic differential cross section we have no way of going to c.m. system because the two different final states are considered simultaneously. Thus $d\sigma^{E+I}/d\Omega$ contains both c.m. and lab variables.

Here we use the formulae given by Ferreira.[14] (The notation used is defined in Appendix D, if not defined in this section.)

$$\frac{d\sigma^{E+I}}{d\Omega} = \frac{Mq_0 J_0}{k^2 E_{q_f} E_{n_f}} \left\{ \frac{d\sigma^p}{d\bar{\Omega}} + \frac{d\sigma^n}{d\bar{\Omega}} + \frac{H_2}{8} \frac{J'_0}{J_0} \left[|3a_1 + a_0 + 2a_c|^2 \right.\right.$$

$$\left.\left. - |a_1 - a_0 + 2a_c|^2 + \frac{1}{3} |3b_1 + b_0|^2 - \frac{1}{3} |b_1 - b_0|^2 \right] \right\},$$

where

$$\frac{d\sigma^p}{d\bar{\Omega}} = |a_1 + a_c|^2 + |b_1|^2 ,$$

$$\frac{d\sigma^n}{d\bar{\Omega}} = \frac{1}{4} \left[|a_1 + a_0|^2 + |b_1 + b_0|^2 \right],$$

$$H^d = \frac{J_0'}{J_0} \left| \int \psi_D^*(r) \exp\left[-\frac{1}{2} i (\bar{q}_0 - \bar{q}_f) \cdot \bar{r} \right] \psi_D(r) \, d\vec{r} \right|^2 ,$$

$$J_0 = \frac{q_f^2}{\frac{q_f}{E_f} - \frac{q_f - q_0 \cos\theta}{E_{n_f}}} ,$$

$$J_0' = \frac{q'^2_f}{\frac{q'_f}{E'_f} - \frac{q'_f - q'_0 \cos\theta}{E'_{n_f}}} ,$$

a_1, a_0, b_1, and b_0 are as given in Eq. (4-2), and a_c is the Coulomb scattering amplitude.

J_0 and J'_0 are defined for the kinematics of $K + n \rightarrow K + n$ and $K + d \rightarrow K + d$, respectively.

In the calculation of the total cross section we pick $\cos\theta$ first, then calculate the corresponding $\cos\overline{\theta}$. Knowing $\cos\overline{\theta}$, we calculate $|f(a,b)|^2$. The rest of the kinematics is then calculated to complete $d\sigma^{E+I}/d\Omega$ at $\cos\theta$. By use of Simpson's Rule, $d\sigma^{E+I}/d\Omega$ is integrated from $\cos\theta = -1$ to $\cos\theta$ cutoff to obtain the total cross section.

B. Phase-Shift Search Program

Our search program, programmed and used on both the IBM 704 and 709 machines, makes use of the method of gradient descent from randomly selected points. Unlike a phase-shift analysis for counter experiments, in which the machine compares the calculated differential cross sections with the measured ones, our analysis of the data given in a histogram requires calculation of

$$\int_{\cos\overline{\theta}_i}^{\cos\overline{\theta}_j} \frac{d\sigma}{d\overline{\Omega}}\, d\overline{\Omega} ,$$

and then comparison of the result with the histogram data. This allows us to choose a number of intervals and widths of $\cos\overline{\theta}$, restricted only by statistics, by accuracy of the measured values of $\cos\overline{\theta}$, and by the number of variables under consideration. In Section IV we discussed how we chose these intervals. The program was written so as to be able to utilize any choice of $\cos\overline{\theta}_i$ to $\cos\overline{\theta}_j$ up to 10 intervals. The variables of the program were also left arbitrary; therefore we may choose phase shifts as variables for each energy or, alternatively, scattering lengths and effective ranges as variables when we analyze a few energies simultaneously. The number of variables was limited to a maximum of ten.

The goodness of fit for a given set of variables to the experimental data was determined by calculating the quantity M, usually referred to as χ^2,

$$M = \sum_i \left| \frac{\int_{\cos\overline{\theta}_i}^{\cos\overline{\theta}_{i+1}} \frac{d\sigma}{d\overline{\Omega}}\, d\overline{\Omega} - \sigma_{i,i+1}}{\Delta\sigma_{i,i+1}} \right|^2 , \qquad \text{(B-1)}$$

where $\sigma_{i,i+1}$ and $\Delta\sigma_{i,i+1}$ are the experimentally measured cross section and its error, respectively, in the interval of $\cos\overline{\theta}_i$ to $\cos\overline{\theta}_{i+1}$ and

$$\int_{\cos\overline{\theta}_i}^{\cos\overline{\theta}_{i+1}} \frac{d\sigma}{d\overline{\Omega}}\, d\overline{\Omega}$$

is given in Appendix D, Eq. (D-12).

The logic of the program is roughly as follows:

(1) Select n random numbers r_i between 0 and 1

$i = 1, 2, \cdots, n$, for $n \leq 10$.

(2) Calculate variables $v_i = v_i^{\min} + (v_i^{\max} - v_i^{\min})r_i$; e.g., when variables are phase shifts we used $v_i^{\min} = -\frac{\pi}{2}$ and $v_i^{\max} = \frac{\pi}{2}$.

(3) Calculate $\Delta M(v_1, v_2, \cdots, v_n) = M(v_1 + \delta, v_2 \cdots, v_n) - M(v_1, v_2, \cdots, v_n)$

and $\Delta M(v_1 + m\delta, v_2, \cdots, v_n) = M[v_1 + (m+1)\delta, v_2, \cdots, v_n]$

$$- M(v_1 + m\delta, v_2, \cdots, v_n),$$

where m and δ are constants initially read into the machine. When the variables are phase shifts we use $\delta = 0.005$ radian, $m = 20.0$.

(4) The signs of $\Delta M(v_1)$ and $\Delta M(v_1 + m\delta)$ are compared; there are four possibilities.

(5)

	Sign $\Delta M(v_1)$	Sign $\Delta M(v_1 + m\delta)$
a	+	+
b	-	-
c	+	+
d	-	+

a. Calculate Sign $\Delta M(v_1 - m\delta)$ and return to beginning of (5) with the replacements

$v_1 - m\delta \rightarrow v_1$

and

$v_1 \rightarrow v_1 + m\delta$.

b. Calculate Sign $\Delta M(v_1 + 2m\delta)$ and return to beginning of (5) with the replacements

$$v_1 + m\delta \rightarrow v_1$$

and

$$v_1 + 2m\delta \rightarrow v_1 + m\delta \ .$$

c or d. Test if a maximum or minimum is trapped. If a maximum is trapped, return to (1). If a minimum is trapped, we pinpoint the minimum as follows:

(6) Replace m by $m/2$ and repeat (3) through (5). Repeat this process p times until $| v_1^{p-1} - v_1^{p} | < n\,\delta$, where n is fixed in advance. Designate this v_1 as $v_1^{(1)}$.

(7) We return to (3), replace v_1 by $v_1^{(1)}$, and go through the above cycle again using v_2 instead of v_1. When we have exhausted the n variables we have a set of new variables $[v_1^{(1)}, v_2^{(1)}, \cdots, v_n^{(1)}]$ that is the first approximation to the solution.

(8) The above is repeated (j+1) times, until the following inequalities hold:

$$|v_1^{(j+1)} - v_1^{j}| \leq \epsilon \ ,$$
$$|v_2^{(j+1)} - v_2^{j}| \leq \epsilon \ ,$$
$$\vdots$$
$$|v_n^{(j+1)} - v_n^{j}| \leq \epsilon \ ,$$

where ϵ is initially read into the machine. The final solution is then

$$[v_1^{(j+1)}, v_2^{(j+1)}, \cdots, v_n^{(j+1)}] \ .$$

C. Error Program

A method involving the error matrix is customarily used to obtain the uncertainty in each phase shift.[22, 23] Such an analysis is based on the assumption that it is a good approximation to expand M only to second order in a Taylor's series centered about the minimum. Note that the first-order term is zero by definition. Consider $(\delta_1, \delta_2 \cdots, \delta_n)$ to be a set of phase shifts that gives rise to a minimum M. Then

$$M(\delta_1+\Delta\delta_1, \delta_2+\Delta\delta_2, \cdots, \delta_n+\Delta\delta_n) \approx M(\delta_1, \delta_2 \cdots, \delta_n) + \sum_{i,j=1}^{n} G_{ij}\Delta\delta_i\Delta\delta_j,$$

$$\Delta M(\delta_1, \delta_2 \cdots, \delta_n) \approx \sum_{ij}^{n} G_{ij}\,\Delta\delta_i\Delta\delta_j\,, \qquad \text{(C-1)}$$

and the error matrix is defined as G^{-1}.

(1) Calculation of G_{ii}.

$$\Delta M(\delta_1, \cdots, \delta_i \pm \Delta\delta_i, \cdots, \delta_n) = \Delta M_{ii}^{\pm}\,,$$

and

$$\left\langle G_{ii} \right\rangle_{av} = \frac{\Delta M_{ii}^{+} + \Delta M_{ii}^{-}}{2(\Delta\delta_i)^2}\,. \qquad \text{(C-2)}$$

In actual calculations $(\delta_1, \delta_2, \cdots, \delta_n)$ might be a few degrees off from the minimum of the nth hypersurface. The absolute value of each ΔM_{ii}^{+} and ΔM_{ii}^{-} was taken in order to ensure that, in case one of them is negative, we may still get a reasonable $\left\langle G_{ii} \right\rangle_{av}$.

(2) Calculation of G_{ij}, $i \neq j$.

$$\Delta M(\delta_1, \cdots, \delta_i \pm \Delta\delta_i, \cdots, \delta_j \pm \Delta\delta_j, \cdots, \delta_n) = \Delta M_{ij}^{\pm\pm}\,,$$

$$\Delta M(\delta_1, \cdots, \delta_i \pm \Delta\delta_i, \cdots, \delta_j \mp \Delta\delta_j, \cdots, \delta_n) = \Delta M_{ij}^{\pm\mp}\,,$$

and

$$\left\langle G_{ij} \right\rangle_{av} = \frac{\Delta M_{ij}^{++} + \Delta M_{ij}^{--} - \Delta M_{ij}^{+-} - \Delta M_{ij}^{-+}}{8\,(\Delta\delta_i)\,(\Delta\delta_j)}\,. \qquad \text{(C-3)}$$

Here again the absolute value of each ΔM_{ij} was taken.

The elements of G^{-1} are related to the uncertainties in the phase shifts. According to statistical theory $\sqrt{(G^{-1})_{ii}} = (\Delta\delta_i)_{rms}$ and $(G^{-1})_{ij} = C_{ij} \times (\Delta\delta_i)_{rms} \times (\Delta\delta_j)_{rms}$, where C_{ij} is the ijth correlation coefficient, with a value between +1 and -1. The correlation coefficients indicate the degree to which the phase shifts are related. For $C_{ij} = 0$, δ_i and δ_j are independent.

When there is a large amount of experimental data, the M hypersurface usually has a very sharp minimum, and the error matrix can be employed. But when good statistics are not available, the M hypersurface may in some cases be fairly flat in the neighborhood of the minimum. If this is the case, $|\Delta M| \to 0$; the error matrix analysis is not applicable.

Our direct error-analysis program, programmed and used for both the IBM 704 and 709 machines, searches for the band of hypersurfaces contained between $M = M_1$ and $M = M_1 + \Delta M$. The logic is as follows:

(a) We start from the set of phase shifts found by the search program for minimum M.

(b) Consider the case of only three phase shifts. We keep two of them fixed and vary the third until it reaches the specified band of M at two places. We then do the same for the other two variables.

Let $(\delta_1, \delta_2, \delta_3)$ be phase shift at minimum M and $\delta_1^{\pm}$, $\delta_2^{\pm}$, $\delta_3^{\pm}$ be phase shift located at the band of M_1 and $(M_1+\Delta M)$ in each direction.

Define $$a_i = \frac{\delta_i^+ + \delta_i^-}{2} ,$$

$$b_i = \frac{\delta_i^+ - \delta_i^-}{2} ,$$

and construct

$$f(\delta_1, \delta_2, \delta_3) = \sum_{i=1}^{3} \left(\frac{\delta_i - b_i}{a_i} \right)^2 .$$

(c) In order to find out how good this ellipsoidal approximation is, we scan that part of the hypersurface bounded by the band of M_1 and $(M_1 + \Delta M)$. If any point on the band is found too far outside the ellipsoid, we print out its position. In practice we print out the position for $f \geq 2$.

D. Impulse and Closure Approximations

We will present a derivation of Eq. (4-3) by the procedure given by FGW. Much of this derivation is given by Ferreira.[16]

Notation

$\vec{q}_0$, $\vec{q}_f$: initial and final K-meson momentum (lab),

$\vec{n}_0$, $\vec{n}_f$: initial neutron and final recoil-proton momentum (lab),

$\vec{p}_0$, $\vec{p}_f$: initial proton and final spectator-proton momentum (lab).

Define

$$\vec{\ell} = \frac{1}{2}(\vec{p} - \vec{n}),$$

$$\vec{L} = \vec{p} + \vec{n},$$

and

$$\vec{s} = \frac{M\vec{q} - E_q \vec{n}}{M + E_q},$$

where $E_q = \sqrt{m^2 + q^2}$, and m and M are the masses of the K meson and the nucleon, respectively.

Let t_{fi} be the transition amplitude for the scattering, then

$$t_{fi} = \langle f|t|i\rangle = \int \langle f|\vec{\ell}'\vec{L}\,\vec{q}'\rangle \langle \vec{q}'\vec{L}'\vec{\ell}'|t_n|\vec{\ell}\,\vec{L}\,\vec{q}\rangle \langle \vec{q}\,\vec{L}\,\vec{\ell}\,|i\rangle \times d\vec{\ell}'d\vec{L}'d\vec{q}'\,d\vec{\ell}\,d\vec{L}\,d\vec{q}\,, \quad \text{(D-1)}$$

$$\langle \vec{q}'\,\vec{L}'\,\vec{\ell}'\,|t_n|\,\vec{\ell}\,\vec{L}\,\vec{q}\rangle = \langle \vec{p}'\,\vec{n}'\,\vec{q}'|t_n|\,\vec{q}\,\vec{n}\,\vec{p}\rangle\,,$$

$$= \delta(\vec{p} - \vec{p}')\,\delta(\vec{n}+\vec{q} - \vec{n}'- \vec{q}')\,\langle \vec{s}'|r_n|\vec{s}\rangle\,,$$

$$= \delta(\vec{L}+\vec{q} - \vec{L}'-\vec{q}')\,\delta(\vec{\ell}-\vec{\ell}' - \tfrac{1}{2}(\vec{q}-\vec{q}'))\times \langle \vec{s}'|r_n|\vec{s}\rangle\,,$$

$$\langle \vec{\ell}'\,\vec{L}'\vec{q}'|f\rangle = \delta(\vec{L}_f-\vec{L}')\delta(\vec{q}_f-\vec{q}')\langle \vec{\ell}'|f\rangle\,,$$

and

$$\langle \vec{\ell}\,\vec{L}\,\vec{q}\,|\,i\rangle = \delta(\vec{L}_0-\vec{L})\,\delta(\vec{q}_0-\vec{q})\,\langle \vec{\ell}\,|\,i\rangle\,.$$

Integrating over all the δ functions, we obtain

$$t_{fi} = \delta(\vec{L}_f + \vec{q}_f-\vec{q}_0)\int \langle f\,|\,\vec{\ell} - \tfrac{1}{2}(\vec{q}_0-\vec{q}_f)\rangle\,\langle \vec{s}'\,|\,r_n\,|\,\vec{s}\rangle\,\langle \vec{\ell}\,|\,i\rangle\,d\vec{\ell}\,.$$

Now we take $\langle \vec{s}'\,|\,r_n\,|\,\vec{s}\rangle$ outside the integral. (See FGW for justification of this.)

$$t_{fi} = \delta(\vec{L}_f + \vec{q}_f - \vec{q}_0) \langle \vec{s}' \mid r_n \mid \vec{s} \rangle I, \qquad \text{(D-2)}$$

where

$$I = \int \langle f \mid \vec{\ell} - \frac{1}{2}(\vec{q}_0 - \vec{q}_f) \rangle \langle \vec{\ell} \mid i \rangle \, d\vec{\ell},$$

$$= \int \langle f \mid \vec{r} \rangle \exp\left[\frac{1}{2} i(\vec{q}_0 - q_f)\cdot \vec{r}\right] \langle \vec{r} \mid i \rangle \, d\vec{r},$$

and

$$\langle \vec{r} \mid i \rangle = \psi_D(\vec{r}) = N\left(\frac{e^{-ar}}{r} - \frac{e^{-\beta r}}{r}\right),$$

$$N^2 = \frac{a\beta(a+\beta)}{2\pi(a-\beta)^2},$$

and

$$\langle \vec{r} \mid f \rangle = \Phi_\ell(\vec{r})$$

The term $\Phi_\ell(\vec{r})$ is the final two-proton wave function with a relative momentum of ℓ. For convenience we calculate the differential cross sections of the singlet and triplet two-proton final states separately. Following the procedure given by FGW, we write

$$\frac{d\sigma^s}{d\Omega} = \frac{(2\pi)^4}{v_K} \int \Sigma' \delta(E_f - E_i) \mid \langle \vec{s}' \mid r_n \mid \vec{s} \rangle \mid^2 \mid I^s \mid^2 q^2 dq \, d\vec{\ell}$$

and

$$\frac{d\sigma^t}{d\Omega} = \frac{(2\pi)^4}{v_K} \int \Sigma' \delta(E_f - E_i) \mid \langle \vec{s}' \mid r_n \mid \vec{s} \rangle \mid^2 \mid I^t \mid^2 q^2 dq \, d\vec{\ell}. \qquad \text{(D-3)}$$

Here Σ' means summing over the final spin and averaging over the initial spin states, so that we obtain

$$\sum_s' \mid \langle \vec{s}' \mid r_n \mid \vec{s} \rangle \mid^2 = \frac{1}{3} \mid r_n^{(2)} \mid^2,$$

and

$$\sum_t' \mid \langle \vec{s}' \mid r_n \mid \vec{s} \rangle \mid^2 = \mid r_n^{(1)} \mid^2 + \frac{2}{3} \mid r_n^{(2)} \mid^2,$$

where

$$r_n = r_n^{(1)} + \vec{\sigma}_n \cdot \vec{r}_n^{(2)}.$$

Equation (D-3) may be written as

$$\frac{d\sigma^s}{d\Omega} = \frac{(2\pi)^4}{v_K} J_0 \left[\frac{1}{3} | r_n^{(2)} |^2 \right] H^s ,$$

and

$$\frac{d\sigma^t}{d\Omega} = \frac{(2\pi)^4}{v_K} J_0 \left[| r_n^{(1)} |^2 + \frac{2}{3} | r_n^{(2)} |^2 \right] H^t , \qquad \text{(D-4)}$$

where

$$H^s = \frac{1}{J_0} \int \delta(E_f - E_i)\, q^2 dq\, d\vec{\ell}\, | I^s |^2 ,$$

$$H^t = \frac{1}{J_0} \int \delta(E_f - E_i)\, q^2 dq\, d\vec{\ell}\, | I^t |^2 \qquad \text{(D-5)}$$

Here

$$I^s = \frac{1}{\sqrt{2}} \int \{ \underline{\Phi}_\ell(\vec{r}) + \underline{\Phi}_\ell(-\vec{r}) \} \exp\left[\frac{1}{2} i(\vec{q}_0 - \vec{q}_f) \cdot \vec{r} \right] \psi_D(r)\, d\vec{r},$$

$$I^t = \frac{1}{\sqrt{2}} \int \{ \underline{\Phi}_\ell(\vec{r}) - \underline{\Phi}_\ell(-\vec{r}) \} \exp\left[\frac{1}{2} i(\vec{q}_0 - \vec{q}_f) \cdot \vec{r} \right] \psi_D(r)\, d\vec{r}, \qquad \text{(D-6)}$$

and

$$J_0 = \int \delta(E_f - E_i)\, q^2\, dq .$$

In Eq. (D-6), the generalized Pauli principle is incorporated for two outgoing protons. If one assumes that all values of ℓ are permissible, then a closure property may be used:

$$\int \underline{\Phi}^*_\ell(\vec{r})\, \underline{\Phi}_\ell(\vec{r}')\, d\vec{\ell} = \delta(\vec{r} - \vec{r}') \qquad \text{(D-7)}$$

The evaluation of H^s and H^t with the aid of Eq. (D-7) is the closure approximation. The closure approximation gives

$$H^s = 1 + H_2$$

and

$$H^t = 1 - H_2 , \qquad \text{(D-8)}$$

where

$$H_2 = \int \psi^*_D(r) \exp\left[-i(\vec{q}_0 - \vec{q}_f) \cdot \vec{r} \right] \psi_D(\vec{r})\, d\vec{r} . \qquad \text{(D-9)}$$

For the derivation of Eq. (4-3), we want to go to the K^+-neutron c.m. system. In order to do this, we note

$\frac{d\vec{p}}{E_p}$ is a Lorentz invariant

and

$$\frac{1}{v_k} = \frac{E_{n_0} E_{q_0}}{\left((E_{q_0} E_{n_0} - \vec{q}_0 \cdot \vec{n}_0)^2 - M^2 m^2 \right)^{1/2}} ,$$

where the denominator is a Lorentz invariant.

By use of the relation $\frac{d\sigma}{d\Omega} d\Omega = \frac{d\sigma}{d\bar{\Omega}} d\bar{\Omega}$, the matrix element is related to the scattering amplitude $M(\bar{\theta})$ by

$$M(\bar{\theta}) = (2\pi)^2 \frac{k_{c.m.}}{v_{c.m.}} \frac{\left(E_{q_f} E_{n_f} E_{q_0} E_{n_0} \right)^{1/2}}{E_{q_{c.m.}} E_{n_{c.m.}}} \langle \vec{s}' | r_n | \vec{s} \rangle . \qquad \text{(D-10)}$$

We obtain

$$\frac{d\sigma^s}{d\bar{\Omega}} = \frac{1}{3} | b(\bar{\theta}) |^2 (1 + H_2) ,$$

$$\frac{d\sigma^t}{d\bar{\Omega}} = \left[| a(\bar{\theta}) |^2 + \frac{2}{3} | b(\bar{\theta}) |^2 \right] (1 - H_2) , \qquad \text{(D-11)}$$

and

$$\frac{d\sigma^{ce}}{d\bar{\Omega}} = \frac{d\sigma^s}{d\bar{\Omega}} + \frac{d\sigma^t}{d\bar{\Omega}} .$$

Here $\frac{d\sigma}{d\Omega} = \frac{d\sigma}{d\bar{\Omega}} \frac{d\bar{\Omega}}{d\Omega}$, and $\frac{d\bar{\Omega}}{d\Omega}$ was calculated for the stationary neutron.

It was stated that the closure approximation is very poor for small momentum transfers because $\Phi_\ell(r)$ and $\psi_D(r)$ are orthogonal;[16] if this is so, Eq. (D-5) should be very small, whereas the approximate one is not. It should be noted, however, that H^t is actually very small for small momentum transfers because of the generalized Pauli principle. H^s does not become small, but the singlet state has a much smaller contribution to the differential cross section than the triplet state; also, the singlet state has a $\sin^2\bar{\theta}$ dependence in the differential cross section that is very small for a small momentum transfer. This is perhaps the reason why the phase-shift analyses with and without the forward data did not differ much.

Equation (D-9) may be integrated to get Eq. (4-5):

$$\int_{\cos\bar{\theta}_i}^{\cos\bar{\theta}_j} \frac{d\sigma}{d\bar{\Omega}} d\bar{\Omega} = \frac{2\pi}{4k^2} \left\{ \left[A\cos\bar{\theta} + \frac{B}{2}\cos^2\bar{\theta} + \frac{C}{3}\cos^3\bar{\theta} + \frac{D}{4}\cos^4\bar{\theta} + \frac{E}{5}\cos^5\bar{\theta} \right]_{\cos\bar{\theta}_i}^{\cos\bar{\theta}_j} + \right.$$

$$+ 4\lambda \left[f\left(zt;\ z = \frac{k}{\alpha}\right) - 2f\left(zt;\ z = \frac{2k}{\alpha+\beta}\right) + f\left(zt;\ z = \frac{k}{\beta}\right) \right]_{t_i}^{t_j} \Bigg\}, \tag{D-12}$$

where

$$t = \sin \frac{\theta}{2} ,$$

$$f(zt) = \frac{A'}{z} \left\{ (zt) \tan^{-1}(zt) - \frac{1}{2} \ln \left[1 + (zt)^2 \right] \right\}$$

$$+ \frac{B'}{z^3} \left\{ \frac{(zt)^3}{3} \tan^{-1}(zt) - \frac{(zt)^2}{6} + \frac{1}{6} \ln \left[1 + (zt)^2 \right] \right\}$$

$$+ \frac{C'}{z^5} \left\{ \frac{(zt)^5}{5} \tan^{-1}(zt) - \frac{(zt)^4}{20} + \frac{(zt)^2}{10} - \frac{1}{10} \ln \left[1 + (zt)^2 \right] \right\}$$

$$+ \frac{D'}{z^7} \left\{ \frac{(zt)^7}{7} \tan^{-1}(zt) - \frac{(zt)^6}{42} + \frac{(zt)^4}{28} - \frac{(zt)^2}{14} + \frac{1}{14} \ln \left[1 + (zt)^2 \right] \right\}$$

$$+ \frac{E'}{z^9} \left\{ \frac{(zt)^9}{9} \tan^{-1}(zt) - \frac{(zt)^8}{72} + \frac{(zt)^6}{54} - \frac{(zt)^4}{36} + \frac{(zt)^2}{18} - \frac{1}{18} \ln \left[1 + (zt)^2 \right] \right\} ,$$

and

$$A' = A + B + C + D + E ,$$

$$B' = -2 (B + 2C + 3D + 4E + 2F + 2G + 2H),$$

$$C' = 4 (C + 3D + 6E + F + 3G + 5H),$$

$$D' = -8 (D + 4E + G + 4H),$$

$$E' = 16 (E + H) ,$$

$$\lambda = \frac{(\alpha + \beta)\ \alpha\beta}{(\alpha-\beta)\ k} ,$$

$$A = | \eta_1 - \eta_0 + \Lambda_{03} + \frac{3}{2} \Lambda_{05} |^2 + | \eta_{01} - \eta_{03} |^2 ,$$

$$B = -2 \text{ Re } (\eta_1 - \eta_0 + \Lambda_{03} + \frac{3}{2} \Lambda_{05})^* (\eta_{01} + 2 \eta_{03}) + 6 \text{ Re } \times (\eta_{01} - \eta_{03})^* (\Lambda_{03} - \Lambda_{05}) ,$$

$$C = - 3 \text{ Re } (\eta_1 - \eta_0 + \Lambda_{03} + \frac{3}{2} \Lambda_{05})^* (2 \Lambda_{03} + 3 \Lambda_{05}) + | \eta_{01} + 2\eta_{03} |^2 - | \eta_{01} - \eta_{03} |^2 + 9 | \Lambda_{03} - \Lambda_{05} |^2 ,$$

$$D = 3 \text{ Re } (\eta_{01} - 2 \eta_{03})^* (2\Lambda_{03} + 3 \Lambda_{05}) - 6 \text{ Re } (\eta_{01} - \eta_{03})^* | \Lambda_{03} - \Lambda_{05}) ,$$

$$E = \frac{9}{4} | 2\Lambda_{03} + 3 \Lambda_{05} |^2 - 9 | \Lambda_{03} - \Lambda_{05} |^2 ,$$

$$F = \frac{2}{3} | \eta_{01} - \eta_{03} |^2 ,$$

$$G = 4 \text{ Re } (\eta_{01} - \eta_{03})^* (\Lambda_{03} - \Lambda_{05}) ,$$

and

$$H = 6 | \Lambda_{03} - \Lambda_{05} |^2 .$$

The first subscript refers to T spin and the second to total angular momentum 2j. Phase shifts of η_0, η_{0j}, and Λ_{0j} refer to the T = 0 S wave, P wave, and D wave, respectively. Here $\eta = e^{i\delta} \sin \delta$, and $\Lambda = e^{i\Delta} \sin \Delta$.

E. S-Wave Fit

E. M. Ferreira reported that a pure S wave in T = 0 is consistent with our data at 356, 530, and 642 Mev/c.[16] He found especially good agreement with our 642-Mev/c data. His calculation differs from his previous one.[14] in that he considers a correction term due to the final proton-proton interaction, including the Coulomb force. The apparent agreement of our data with his calculations for the pure S wave in the T = 0 amplitude seems to lie in the way our data were plotted, that is, the agreement comes mainly from the backward laboratory-system angular distributions where there are only very few events in each interval. In Fig. 14 we have taken his angular distributions and transformed them to the c. m. system, neglecting the initial neutron momentum. The solid lines in Fig. 14 correspond to his recent work, in which the final proton-proton interaction was considered, and the dotted lines correspond to his previous work, in which the closure approximation was used. The same phase shift was used in both calculations. We see that his recent work, which apparently agreed with our data in the laboratory system, fails to do so in the c. m. system. We also note that his new calculation and the old differ increasingly as the incident energy becomes higher. This suggests that the final-state interaction becomes more and more important as the incident energy increases.

In his calculation, the matrix element $\langle \vec{s}' \mid r_n \mid \vec{s} \rangle$ was related to the scattering amplitude $M(\theta)$ for the nonrelativistic case. That is, instead of Eq. (D-10), he used

$$M(\theta) = (2\pi)^2 \frac{mM}{m + M} \langle \vec{s}' \mid r_n \mid \vec{s} \rangle . \qquad \text{(E-1)}$$

Note that Eq. (D-10) reduces to Eq. (E-1) in the nonrelativistic limit. The 500-Mev/c to 900-Mev/c K^+ mesons can hardly be treated nonrelativistically. This is perhaps the reason why the forward angular region is more enhanced as the momentum of the K^+ meson increases.

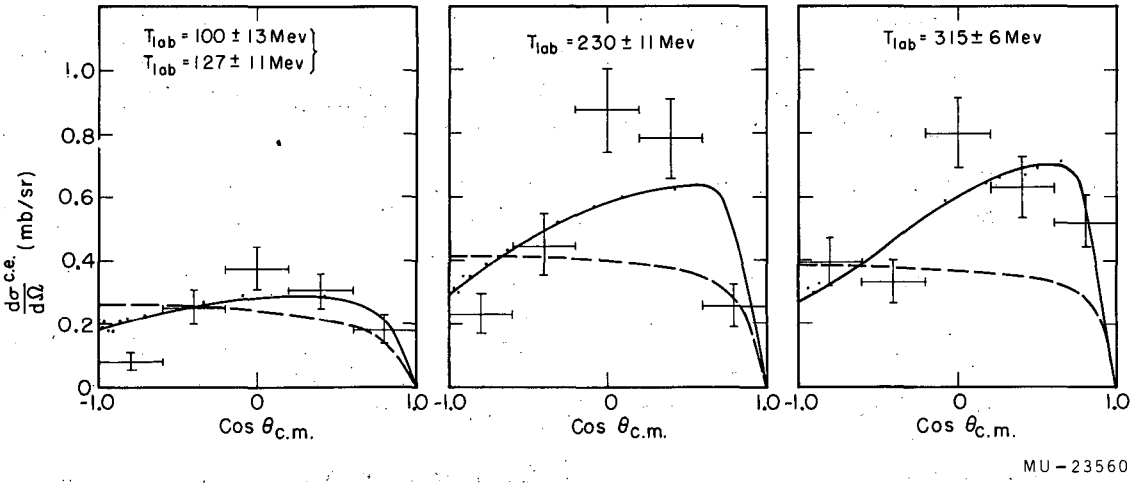

Fig. 14. Comparison of Ferreira's work with our data, at 100 and 127 Mev combined, 230, and 315 Mev. Solid lines correspond to his recent work in which the final proton-proton interaction was considered, and the dotted lines correspond to his previous work in which the closure approximation was used.

REFERENCES

1. G. Goldhaber, S. Goldhaber, J. Kadyk, T. Stubbs, D. Stork, and H. Ticho, Bevatron Internal Report 483 (1960) (unpublished).

2. P. Eberhard, M. Good, and H. Ticho, Rev. Sci. Instr. 31, 1054 (1960).

3. W. Humphrey, Lawrence Radiation Laboratory Alvarez-Group Memo 115 (1959) (unpublished).

4. P. Berge, Lawrence Radiation Laboratory Alvarez-Group Memo 86 (1960) (unpublished).

5. W. Chinowsky, G. Goldhaber, S. Goldhaber, W. Lee, T. O'Halloran, T. Stubbs, W. Slater, D. Stork, and H. Ticho, in Proceedings of the 1960 Annual International Conference on High Energy Physics at Rochester (Interscience Publishers Inc., New York, 1960), p. 451.

6. F. Crawford, Jr., M. Cresti, R. Douglass, M. Good, G. Kalbfleisch, M. Stevenson, and H. Ticho, Phys. Rev. Letters 2, 266 (1959).

7. T. Kycia, L. Kerth, and R. Baender, Phys. Rev. 118, 553 (1960).

8. T. Stubbs, S. Goldhaber, H. Bradner, W. Chinowsky, G. Goldhaber, W. Lee, T. O'Halloran, W. Slater, D. Stork, and H. Ticho, Bull. Am. Phys. Soc., Series I, 6, 291 (1961).

9. See, for example, B. Zorn and G. Zorn, Phys. Rev. 120, 1898 (1960); M. Melkanoff, D. Prowse, D. Stork, and H. Ticho, Phys. Rev. Letters 5, 108 (1960).

10. G. Chew, Phys. Rev. 80, 196 (1950).

11. R. Rockmore, Phys. Rev. 105, 256 (1957).

12. S. Fernbach, T. Green, and K. Watson, Phys. Rev. 84, 1084 (1951).

13. K. Rogers and L. Lederman, Phys. Rev. 105, 247 (1957).

14. E. Ferreira, Phys. Rev. 115, 1727 (1959).

15. M. Gourdin and A. Martin, Nuovo cimento 11, 670 (1959).

16. E. Ferreira, Ph. D. Thesis, University of London, 1961 (unpublished).

17. M. Gourdin and A. Martin, Nuovo cimento 14, 722 (1959).

18. L. Hulthén and A. Sugawara, Handbuch der Physik, Vol. XXXIV (Springer-Verlag, Berlin, 1957).

19. T. Day, L. Rodberg, G. Snow, and J. Sucher, Nuovo cimento XVI, 770 (1960).

20. Benjamin W. Lee, Study of K^+-N Scattering in the Double Dispersion Representation (Ph. D. Thesis), University of Pennsylvania, 1960 (unpublished).

21. F. Ferrari, G. Frye, and M. Pusterla, Phys. Rev. Letters 4, 615 (1960).

22. James Foote, Scattering of Positive Pions on Protons at 310 Mev: Recoil-Nucleon Polarization and Phase-Shift Analysis (Ph. D. Thesis), Lawrence Radiation Laboratory Report UCRL-9191, September 16, 1960 (unpublished).

23. H. Anderson, W. Davidon, M. Glicksman, and U. Kruse, Phys. Rev. 100, 279 (1955).